Available online at www.sciencedirect.com

ScienceDirect

Geochimica et Cosmochimica Acta 245 (2019) 16–34

Geochimica et Cosmochimica Acta

www.elsevier.com/locate/gca

New age and geochemical data from the Walvis Ridge: The temporal and spatial diversity of South Atlantic intraplate volcanism and its possible origin

S. Homrighausen [a,*], K. Hoernle [a,b], F. Hauff [a], J.-A. Wartho [a], P. van den Bogaard [a], D. Garbe-Schönberg [b]

[a] GEOMAR Helmholtz-Zentrum für Ozeanforschung Kiel, Wischhofstr. 1-3, 24148 Kiel, Germany
[b] Institut für Geowissenschaften, Christian-Albrechts Universität zu Kiel, Ludewig-Meyn-Str. 10, 24118 Kiel, Germany

Received 2 February 2018; accepted in revised form 4 September 2018; available online 15 September 2018

Abstract

Long-lived spatial geochemical zonation of the Tristan-Gough and Discovery hotspot tracks and temporal variations from EMI-type basement to HIMU-type late-stage volcanism at the Walvis Ridge and Shona hotspot tracks point to a complex evolution and multiple source areas for the South Atlantic hotspots. Here we report $^{40}Ar/^{39}Ar$ age and geochemical (major and trace element, Sr-Nd-Pb-Hf isotope) data for samples from 16 new sites on the Walvis Ridge. This aseismic ridge is the oldest submarine expression of the Tristan-Gough mantle plume and represents the initial reference locality of the EMI end member in the South Atlantic Ocean. The EMI-type lavas display an excellent age progressive trend of ~31 mm/a along the entire Tristan-Gough hotspot track, indicating constant plate motion over a relatively stationary melt anomaly over the last ~115 Ma. The Gough-type EMI composition of the Tristan-Gough hotspot track is the dominant composition of the >70 Ma part of the Walvis Ridge, the Etendeka and Parana flood basalts, and along the Gough sub-track, extending from DSDP Site 525A on the SW Walvis Ridge to Gough Island, whereas Tristan-type EMI dominates on the Tristan sub-track, extending from DSDP Sites 527 and 528 to Tristan da Cunha Island. Gough-type EMI is also the dominant composition of the northern Discovery and Shona hotspot tracks, suggesting that these hotspots tap a common source reservoir. The continuous EMI-type supply over ≥132 Ma, coupled with high $^{3}He/^{4}He$ (>10 R_A), points to a deep-seated reservoir for this mantle material. The Tristan and Southern Discovery EMI-type flavors can be reproduced by mixing of the Gough-type component with (1) FOZO/PREMA to produce Tristan-type lavas, and (2) marine sediments or upper continental crust to generate the Southern Discovery-type composition. South Atlantic hotspots with EMI-type compositions overlie the margin (1% ∂V_s velocity contour) of the African Large Low Shear Velocity Province (LLSVP), which may promote the emergence of geochemical "zonation". The St. Helena HIMU-type volcanism, however, is located above internal portions of the LLSVP, possibly reflecting a layered LLSVP.

Keywords: Walvis Ridge; Isotope geochemistry; $^{40}Ar/^{39}Ar$ dating; DUPAL-anomaly; EMI mantle end member; HIMU

1. INTRODUCTION

The Tristan-Gough, Discovery and Shona (also referred to as Meteor) volcanic tracks form the most prominent bathymetric features on the South Atlantic seafloor

* Corresponding author.
E-mail address: shomrighausen@geomar.de (S. Homrighausen).

https://doi.org/10.1016/j.gca.2018.09.002
0016-7037/

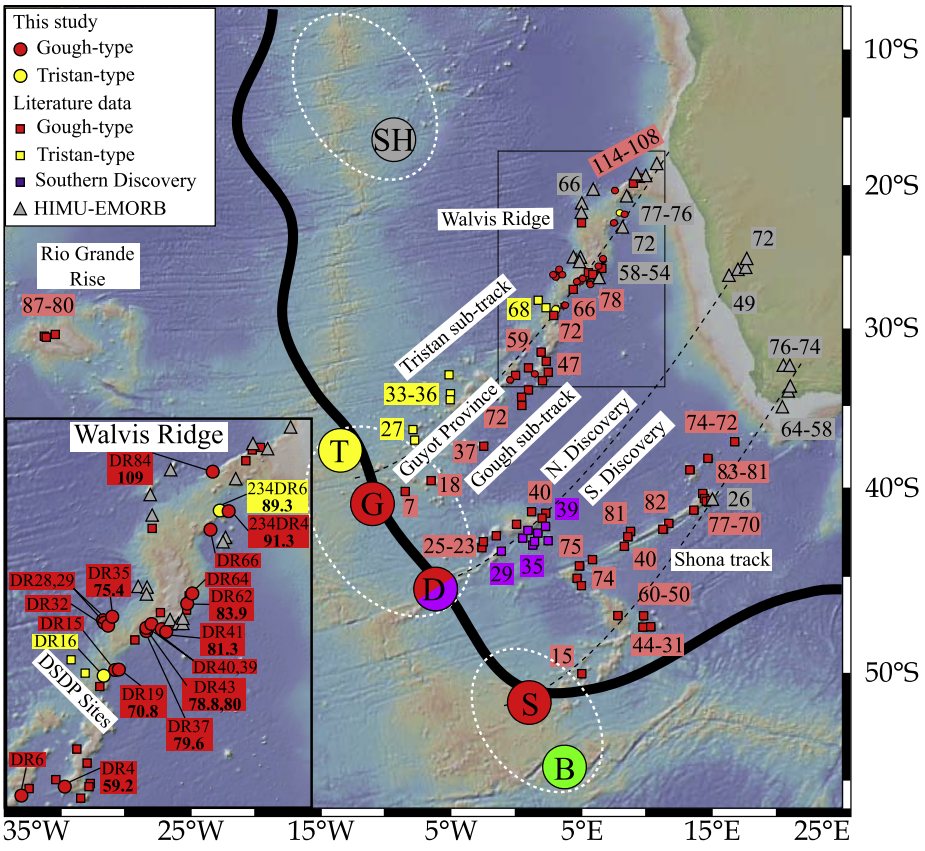

Fig. 1. Map of the South Atlantic showing: (1) the proposed hotspot locations (large circles with SH = St. Helena, T = Tristan, G = Gough, D = Discovery, S = Shona and B = Bouvet), (2) new sample sites from Walvis Ridge SO233 and SO234 cruises (red circles), (3) $^{40}Ar/^{39}Ar$ ages (Ma; Rohde et al., 2013b; O'Connor and Jokat, 2015a, b; Homrighausen et al., 2018a, and this study), (4) the proposed hotspot tracks (dashed black lines; O'Connor and Duncan, 1990; O'Connor et al., 2012), (5) approximate locations of broad low velocity anomalies extending from the base of the lower mantle to depths as shallow as ~1000 km (dashed white circles; French and Romanowicz, 2014) and (6) the 1% ∂V_s contour (thick black line) defining the western margin of the African Large Low Shear Velocity Province (LLSVP; Torsvik et al., 2006). The background color of the ages is related to the different geochemical signatures (yellow = Tristan-type, red = Gough-type, purple = Southern Discovery-type, green = PREMA/FOZO, grey = HIMU-type). The yellow circle with "T" in it represents the location of the Tristan hotspot (or plume conduit), based on the location of the "low-velocity" anomaly in the upper mantle SW of Tristan da Cunha Island (Schlömer et al., 2017). Sample sites of South Atlantic intraplate lavas from the literature are shown as rectangles for EMI-types and triangles for HIMU-EMORB-types. The inset map shows the Walvis Ridge with new sample locations and new $^{40}Ar/^{39}Ar$ age data. Source of bathymetric map: http://www.geomapapp.org. Sources of literature data in this and the following figures: Tristan-Gough system (Le Maitre, 1962; Richardson et al., 1982; Weaver et al., 1987; Le Roex et al., 1990; Cliff et al., 1991; Willbold and Stracke, 2006; Class and le Roex, 2008; Salters and Sachi-Kocher, 2010; Willbold and Stracke, 2010; Rohde et al., 2013a, 2013b; Hoernle et al., 2015; O'Connor and Jokat, 2015a, b), St. Helena (Weaver et al., 1987; Chaffey et al., 1989; Willbold and Stracke, 2006, 2010; Kawabata et al., 2011; Salters et al., 2011; Hanyu et al., 2014), Mid-Atlantic Ridge (MAR; Class and Lehnert, 2012), Discovery Seamounts (Schwindrofska et al., 2016), Shona track (O'Connor et al., 2012; Hoernle et al., 2016), Bouvet (Sun, 1980) and West African HIMU-type lavas (Sun, 1980; Cooper and Reid, 1998; Davies et al., 2001; Janney et al., 2002; Luchs et al., 2013). (For interpretation of the references to colour in this figure legend, the reader is referred to the web version of this article.)

(Fig. 1). These age-progressive volcanic chains (Fig. 1) and southern South Atlantic and western Indian Ocean Mid-Ocean Ridge Basalts (MORBs) have an enriched mantle (EM) type composition (Zindler and Hart, 1986), characterized by high $^{87}Sr/^{86}Sr$, $^{207}Pb/^{204}Pb$ and $^{208}Pb/^{204}Pb$ ratios at a given $^{206}Pb/^{204}Pb$ ratio (or high $\Delta 7/4Pb$ and $\Delta 8/4Pb$ respectively; Hart, 1984), low $^{143}Nd/^{144}Nd$ and $^{176}Hf/^{177}Hf$ ratios, and low to intermediate $^{206}Pb/^{204}Pb$ isotope ratios. This Southern Hemisphere enriched anomaly is referred to as the DUPAL anomaly (Hart, 1984).

Other intraplate lavas in the South Atlantic (Fig. 1) have radiogenic Pb and intermediate Sr-Nd-Hf isotope ratios. St. Helena Island represents the Atlantic type locality for the HIMU (high time-integrated $\mu = {}^{238}U/^{204}Pb$ ratio) end member with a very radiogenic Pb isotopic composition (Zindler and Hart, 1986). On the other hand, Bouvet Island has intermediate Sr-Nd-Pb-Hf isotope ratios and is located at the enriched end of the MORB array, but has slightly more radiogenic Sr and Hf isotope ratios compared to HIMU. This intermediate compositional range has been

"referred to" as PREMA (PREvalent Mantle; Wörner et al., 1986; Zindler and Hart, 1986; Stracke, 2012), FOZO (FOcal Zone; Hart et al., 1992; Stracke et al., 2005) or C (Common component; Hanan and Graham, 1996). PREMA, FOZO and C largely overlap in multiple-isotope space and may be derived from similar source material (see Stracke et al., 2005; Stracke, 2012). Although PREMA can describe this "ubiquitous" common component, we use FOZO/PREMA henceforth, because most authors working in the South Atlantic have referred to it as FOZO in the past (e.g. Gibson et al., 2005; Salters and Sachi-Kocher, 2010).

The NE-SW-oriented submarine volcanic chains associated with the islands of St. Helena, Tristan da Cunha and Gough, as well as the Discovery and Shona volcanic tracks, are consistent with having formed by the NE movement of the African plate over relatively stationary (or synchronously moving) hotspots or mantle plumes (Fig. 1) (O'Connor and le Roex, 1992; O'Connor et al., 2012). Low-velocity seismic anomalies are located in the shallow and deeper mantle beneath St. Helena, Tristan-Gough and Bouvet Islands, as well as the young (SW) ends of the Discovery and Shona volcanic tracks (e.g., Montelli et al., 2006; Zhao, 2007; French and Romanowicz, 2015). High $^{3}He/^{4}He$ ratios (>10 R_A or >10 times the atmospheric He ratio; Sarda et al., 2000; Stroncik et al., 2017) in lavas related to these hotspots (i.e., Etendeka flood basalts and enriched MORB adjacent to the Discovery, Shona and Bouvet hotspots) provide support for the derivation of the material in these hotspots from the lower mantle.

Although the respective seamount chains show many characteristic features of a hotspot or mantle plume (Morgan, 1971; Richards et al., 1989), there are several contradictory observations. Lavas from the Walvis Ridge, for example, have ages up to 40 Ma younger than expected from the linear age progression through the oldest lavas of the Tristan-Gough hotspot track (O'Connor and Duncan, 1990; Rohde et al., 2013b; O'Connor and Jokat, 2015a; Homrighausen et al., 2018a). These young, henceforth referred to as late-stage Walvis, lavas were recovered from seamounts on or near the Walvis Ridge. Notably, these alkalic lavas have a distinct St. Helena HIMU-like incompatible-element and isotopic composition, compared to the primarily tholeiitic EMI-type composition of the flat-top (eroded) main volcanic edifices of the Walvis Ridge (Homrighausen et al., 2018a, 2018b), which we refer to as Walvis basement henceforth. Likewise St. Helena type HIMU late-stage volcanism (e.g. post-dating erosion to form the Richardson guyot-type seamount; Homrighausen et al., 2018b) also occurs on the EMI-type Shona hotspot track (O'Connor et al., 2012; Homrighausen et al., 2018b).

Spatial geochemical zonation has been identified in the Tristan-Gough (since ~70 Ma) and the Discovery (since ~40 Ma) seamount chains (Rohde et al., 2013a; Hoernle et al., 2015; Schwindrofska et al., 2016 Fig. 1). Based on variable $^{207}Pb/^{204}Pb$ ratios, but on uniformly high $^{208}Pb/^{204}Pb$ ratios at a given $^{206}Pb/^{204}Pb$ value, three distinct EMI-type compositional domains (Gough, Tristan, Southern Discovery) have been identified belonging to the South Atlantic DUPAL-anomaly (Rohde et al., 2013a; Hoernle et al., 2015; Schwindrofska et al., 2016). The spatial geochemical zonation of hotspot tracks has been explained by volcanism over: (1) an axially-asymmetric, bi- or tri-laterally-zoned plume conduit that preserves heterogeneities sampled at the base of the plume through laminar flow (e.g., Hoernle et al., 2000; Harpp and White, 2001; Farnetani and Hofmann, 2009; Lohmann et al., 2009; Huang et al., 2011; Weis et al., 2011; Farnetani et al., 2012; Rohde et al., 2013a; Hoernle et al., 2015; Harrison et al., 2017), or (2) a plume consisting of enriched fertile lithologies (e.g., pyroxenite/eclogite) within a relatively depleted peridotitic matrix with lateral variations in melting conditions (temperature/pressure) and referred to as the "plume pudding model" (e.g., Bianco et al., 2008, 2011; Jones et al., 2016, 2017). Both proposed models, however, are controversial and there are several observations inconsistent with these models (e.g., Hofmann and Farnetani, 2013; Hoernle et al., 2015; Jones et al., 2016; Schwindrofska et al., 2016; and discussed below). Overall, it remains unclear as to how the various EMI-types in the South Atlantic are related. We will address several questions related to this geochemical heterogeneity here. These include: Does the EMI-type material come from a source, which shares a common origin and what are possible explanations for the complex spatial and temporal geochemical variability in the South Atlantic intraplate volcanism?

In order to test if the Walvis Ridge basement displays an age progression and to contribute to understanding the complex magmatic evolution of the South Atlantic intraplate volcanism, we report new $^{40}Ar/^{39}Ar$ age and geochemical (major and trace element, Sr-Nd-Pb-Hf isotope) data from the Walvis Ridge. The Walvis Ridge is the oldest submarine expression of the proposed Tristan-Gough hotspot track and represents the EMI-type locality (DSDP Site 525A) in the South Atlantic (Zindler and Hart, 1986). Due to the previous sparse sampling (only 5 sample sites, spread over 1500 km, produced valid $^{40}Ar/^{39}Ar$ ages; Rohde et al., 2013b; O'Connor and Jokat, 2015a, 2015b), the age progression and the history of possible geochemical zonation of the Walvis Ridge remained poorly constrained. In this study we re-evaluate the origin of the Walvis Ridge, and the geochemical variability of intra-plate volcanism in the South Atlantic Ocean.

2. GEOLOGICAL BACKGROUND

Prior to the break-up of Gondwana, the southern and western margins of Gondwana were affected by long-lived subduction zones (Torsvik et al., 2012 and references therein). Whether or not the break-up of Africa and South America was initiated by the arrival of the proposed Tristan-Gough mantle plume is controversial, but consistent with the hotspot (mantle plume) model (e.g., Wilson, 1963; Morgan, 1971; Richards et al., 1989), the Tristan-Gough hotspot track began with the eruption of the Parana-Etendeka continental flood basalt provinces (135–132 Ma, Renne et al., 1996; Renne, 2015). After the separation of South America and Africa, the Walvis Ridge and Rio Grande Rise were formed by the interaction of the plume tail with the newly formed Mid-Atlantic Ridge (MAR;

e.g., Humphris and Thompson, 1983; O'Connor and Duncan, 1990; Rohde et al., 2013a; O'Connor and Jokat, 2015b). Between 80–60 Ma, several major ridge jumps separated the Rio Grande Rise from the Walvis Ridge (Humphris and Thompson, 1983; O'Connor and Duncan, 1990). At the southwestern end of the Walvis Ridge, the Tristan-Gough track bifurcates at ~70 Ma (Rohde et al., 2013b; O'Connor and Jokat, 2015a, 2015b), forming two separate volcanic tracks leading to the active volcanic islands of Tristan da Cunha and Gough, termed the Tristan and Gough sub-tracks (Fig. 1). The two sub-tracks show distinct EMI-type flavors (Rohde et al., 2013a; Hoernle et al., 2015). Lavas from the Gough sub-track have higher $^{207}Pb/^{204}Pb$ ratios, but similar $^{208}Pb/^{204}Pb$ ratios at a given $^{206}Pb/^{204}Pb$ ratio. Their $^{143}Nd/^{144}Nd$ and $^{176}Hf/^{177}Hf$ ratios extend to lower and their $^{87}Sr/^{86}Sr$ ratios to higher values compared to those of the Tristan sub-track. Thus far, only the Gough-type EMI composition has been documented northeast of the DSDP sites (sites 525A, 527 and 528; Rohde et al., 2013a; Hoernle et al., 2015), which form a transect across the southwestern end of the Walvis Ridge (Fig. 1). Therefore, it seems that the Tristan and Gough compositional domains have co-existed since at least 70 Ma (Salters and Sachi-Kocher, 2010; Rohde et al., 2013a; Hoernle et al., 2015).

Although the Tristan-Gough volcanic track shows many characteristic features of a classical mantle plume (e.g., Courtillot et al., 2003), the validity of all but one of the older age dates (O'Connor and Duncan, 1990; O'Connor and le Roex, 1992) were questioned (Baksi, 2007), placing an age progression and thus also a hotspot/plume origin into question. As an alternate model, for example, it has been suggested that the Walvis Ridge developed along deformation zones that penetrated short distances into the plate from the MAR (Fairhead and Wilson, 2005). In their model, the volcanism is mainly triggered by episodic stress release. More recent studies, however, support an age progression for the young SW portion of the Tristan-Gough hotspot track, referred to as Guyot Province (Rohde et al., 2013b; O'Connor and Jokat, 2015a).

3. ANALYTICAL METHODS

The analytical procedures for the $^{40}Ar/^{39}Ar$ age dating and determination of the major and trace element contents and radiogenic isotope ratios are described in detail in Appendix A and all data are reported in Appendices B and C.

4. RESULTS

New samples were obtained from the Walvis Ridge during the SO233 and SO234 cruises of R/V Sonne at depths of 1900–4000 m by dredging: (1) the steep scarps on the margins of the ridge and the walls of cross-cutting graben systems on the top of the plateau; (2) three neighboring seamounts along the eastern margin of the ridge; and (3) two seamounts in the Guyot Province (Fig. 1). A detailed description of the sample localities is given in Hoernle et al. (2014) and Werner and Wagner (2014).

4.1. $^{40}Ar/^{39}Ar$ dating

We report 12 new $^{40}Ar/^{39}Ar$ step-heating ages from 10 different sample sites using hydrofluoric acid-leached feldspar separates and one glass sample (dredge sample SO234 DR6-1). A detailed description of the $^{40}Ar/^{39}Ar$ ages, age spectra and inverse isochron plots are shown in Appendix A, the analyses tables and plots are shown in Appendix C, and the results are outlined in Table 1. Since submarine lavas are affected by variable degrees of alteration, we monitored the Ca/K ratios for mineralogical variations, and the % atmospheric ^{40}Ar ($^{40}Ar_{atm}$) and either the $^{36}Ar/^{39}Ar$ K-feldspar and basalt, or $^{36}Ar/^{37}Ar$ plagioclase alteration index (AI) values. The $^{40}Ar/^{39}Ar$ step-heating age spectra of our samples generally preserve low-temperature steps yielding higher AI values (i.e., above the $^{36}Ar/^{37}Ar$ plagioclase and $^{36}Ar/^{39}Ar$ K-feldspar AI cut-off values of 0.00006, and the $^{36}Ar/^{39}Ar$ basalt AI cut-off value of 0.0006; Baksi, 2007; van den Bogaard, 2013), higher % $^{40}Ar_{atm}$ values, and variable Ca/K ratios relative to the relatively undisturbed medium- to high-temperature steps (Appendix C). This observation indicates that the low-temperature steps are affected by degassing of altered material compared to the fresh medium- and high-temperature steps. Inverse isochron ages were calculated to confirm both the plateau/pseudo-plateau/weighted mean ages and identify if the samples preserved initial atmospheric $^{40}Ar/^{36}Ar$ ratios, without the presence of extraneous ^{40}Ar components. In the majority of samples, the inverse isochron ages of the plateau steps overlap within 95% confidence (conf.) levels of the calculated plateau ages, and yield initial $^{40}Ar/^{36}Ar$ ratios within 95% conf. levels of the atmospheric $^{40}Ar/^{36}Ar$ ratio (Table 1; Appendix C).

4.2. Alteration and age correction of radiogenic isotope ratios

The recovered submarine rocks from the Walvis Ridge have experienced variable degrees of seawater alteration. Even though the freshest parts of the lavas were selected, crushed, and washed with deionized water in an ultrasound bath and then carefully handpicked to obtain the freshest pieces under a binocular microscope (0.5–1 mm size fraction), it was not possible to completely remove all altered material from the samples that were analyzed due to pervasive effects of groundmass alteration. Overall, the loss-on-ignition (LOI), a common indicator for the degree of alteration, is relatively low for such old submarine rocks (LOI < 4.0 wt.% for 28 of the 38 samples). During low temperature seawater alteration, the high field strength elements (e.g., Ti, Zr, Hf, Nb, Ta), Th and rare earth elements (REE) are relatively immobile, whereas the large ion-lithophile elements (e.g., Rb, K, Sr) and U are highly mobile in low-temperature fluids and Pb is mobile in hydrothermal fluids (e.g., Jochum and Verma, 1996). If we exclude the samples with LOI values of >4.0 wt.%, we obtain a reasonably good correlation coefficient for immobile vs. immobile element concentrations (e.g., Nb vs. Zr, Ba, La and Th with the best fit line (R^2) value of 0.86–0.92, not shown) and immobile vs. mobile element concentrations (e.g., Nb vs. Rb, Sr, U and Pb with $R^2 = 0.70–0.78$,

Table 1
$^{40}Ar/^{39}Ar$ step-heating results from the Walvis Ridge.

Cruise	Sample	Phase	Plateau age (Ma ± 2σ)	Cum. % ^{39}Ar	MSWD	P	Steps	Inverse isochron age (Ma ± 95% conf.)
SO233	DR 4-1	K-feld	59.17 ± 0.20	91.8	0.51	0.90	2–13	59.14 ± 0.23
SO233	DR 19-1A	Plag	70.84[a] ± 0.28	41.9	0.83	0.48	9–12	71.20 ± 0.47
SO233	DR 35-12	Plag	75.4 ± 1.2	55.4	1.6	0.15	6–11	76.3 ± 2.6
SO233	DR 41-2	Plag	81.31 ± 0.21	94.7	0.82	0.62	5–16	81.27 ± 0.27
SO233	DR 43-3	Plag	78.84 ± 0.50	51.9	2.0	0.06	9–15	No isochron
SO233	DR 43-6	Plag	80.00 ± 0.52	89.5	0.96	0.49	5–18	79.86 ± 0.71
SO233	DR 62-1	Plag	83.85 ± 0.48	52.1	1.4	0.21	8–16	87.4 ± 1.0
SO233	DR 62-2	Plag	84.2 ± 1.2	57.1	1.3	0.24	2.9	84.2 ± 2.0
WMA	DR62-1/-2		83.90 ± 0.45		0.29	0.59		
SO233	DR 84-2	P/K	109.0[a] ± 1.0[b]	48.0	3.8	0.00	7–16	109.1 ± 2.5
SO234	DR 4-1	Plag	91.34 ± 0.34	66.6	2.2	0.03	4–11	91.24 ± 0.57
SO234	DR 6-1	Glass	89.33 ± 0.20	87.4	0.79	0.69	4–19	89.01 ± 0.27
SO233	DR37-1A	Plag	79.59[c] ± 0.72		2.0	0.07	8–10 & 12–14	80.4 ± 2.1

Abbreviations: Plag = plagioclase; K-feld = K-feldspar; P/K = plagioclase/K-feldspar mixture; Cum. = cumulative; MSWD = Mean Squares Weighted Deviation; P = probability; [a] = pseudo-plateau age (40–50% ^{39}Ar); [b] = 95% conf. error, and [c] = weighted mean age.

not shown). The correlations indicate that secondary processes have not completely altered the fluid mobile element concentrations of the samples. Nevertheless, to minimize the effects of seawater alteration, we focus on immobile elements and radiogenic isotope ratios in this study.

Correction for radiogenic ingrowth since eruption, followed by projection to a common age, is necessary to compare radiogenic isotope ratios of samples with varying emplacement ages, especially when dealing with volcanic rocks formed over an age range of ~135 Ma (see Figs. A1 and A2 in Appendix A). After calculating the initial isotope ratios, we projected them to a common age of 60 Ma, using the proposed EMI source ratios of Willbold and Stracke (2006).

In general, we analyzed 150–200 mg whole-rock chips leached with 2 N HCl at 70 °C for one hour to remove potential surface contamination. The Sm-Nd and Lu-Hf isotope systems are generally resistant to low-temperature alteration and thus the initial isotope ratios should be close to those of the magmatic sources. In contrast, the Sr isotope ratios can be significantly elevated by addition of, or exchange with, seawater Sr (with $^{87}Sr/^{86}Sr$ ratios of ~0.707–0.709 over the last 130 Ma; Jones and Jenkyns, 2001 and references therein). Therefore, rock powders, leached in 6 N HCl at 150 °C for 3 days and then triple rinsed in 18.2 MΩ deionized water, were additionally analyzed for all samples. Twenty-three out of 32 samples produced slightly to significantly lower $^{87}Sr/^{86}Sr$ ratios for the strongly leached powders compared to the mildly leached chips, whereas 8 leached powders yielded slightly higher Sr isotope ratios compared to the chips. We assume that the lowest $^{87}Sr/^{86}Sr$ values from pairs of powder and chips are closest to the magmatic values, and thus we use them for the petrogenetic interpretation. The relatively good correlation of $^{87}Sr/^{86}Sr_{initial}$ vs. $^{143}Nd/^{144}Nd_{initial}$ ($R^2 = 0.71$, not shown) and $^{176}Hf/^{177}Hf_{initial}$ ($R^2 = 0.65$, not shown) compared to initial Nd vs. Hf ($R^2 = 0.60$, not shown), suggests that the initial $^{87}Sr/^{86}Sr$ ratios are representative of the primary magmatic ratios.

The Pb isotope ratios are essential to discriminate between the Tristan- and Gough-type components (Rohde et al., 2013a; Hoernle et al., 2015). Although Th is highly immobile, U is mobile even during low-temperature seafloor alteration and is generally absorbed from seawater, whereas both U and Pb can be mobilized by hydrothermal fluids. Fresh lavas (LOI < 2 wt.%) from the entire Tristan-Gough hotspot track have Nd/Pb ratios of 12 ± 3 (n = 121; 1 standard deviation (SD); Le Maitre, 1962; Richardson et al., 1984; Thompson and Humphris, 1984; Le Roex, 1985; Weaver et al., 1987; Le Roex et al., 1990; Cliff et al., 1991; Gibson et al., 2005; Willbold and Stracke, 2006; Class and le Roex, 2008; Salters and Sachi-Kocher, 2010; Rohde et al., 2013a; Hoernle et al., 2015), which is similar to the Nd/Pb ratios of our samples (12 ± 3; 1 SD; Fig. A3 in Appendix A). Since Nd is relatively immobile during seafloor alteration, we assume that the Pb concentrations in our samples are also close to the primary magmatic values (Fig. A3 in Appendix A). Although within errors, the average Th/U and Nb/U ratios of fresh Tristan-Gough hotspot seamount lavas (Th/U = 4.7 ± 0.7; Nb/U = 43 ± 7; n = 121; LOI < 2 wt.%; same references as for Nd/Pb) compared to our samples (Th/U = 4.2 ± 1.7; Nb/U = 35 ± 16; Fig. A3 in Appendix A) may reflect U uptake in some of our lavas. Nevertheless, if the U uptake took place shortly after the emplacement of the volcanic rocks, and the rock became a closed system thereafter, for example due to a reduction in permeability, the calculated initial $^{206}Pb/^{204}Pb$ and $^{207}Pb/^{204}Pb$ isotope ratios using the measured U-Pb concentrations should reflect those of the source (as demonstrated, for example, by Hauff et al. (2000)). On the other hand, U mobilization occurring long after emplacement of the volcanic rocks will result in over- or under-correction of initial uranogenic Pb isotope ratios. If the lavas were affected relatively recently, the long-term U concentration for each sample can be estimated from the Th/U ratios of the freshest lavas of the Tristan-Gough track (4.7 ± 0.7). The estimated U concentrations can then be used to calculate the initial uranogenic

Pb isotope ratios (e.g., Nobre Silva et al., 2013; Harrison et al., 2017). Since we are unaware of the exact process of U mobilization (e.g., timing, single or multiple event(s) and/or progressive process), we use the calculated $^{206}Pb/^{204}Pb_{60Ma}$ ratios of the measured and normalized U concentration to delimit the maximum over- or under-correction (Appendix A; Fig. A1). The Pb isotope data derived from the two approaches show similar trends for the Tristan-Gough hotspot track and thus we believe that our initial Pb isotope data can be used to make inferences about the isotopic source compositions of the lavas (Fig. A1 in Appendix A). In this study, we use the initial Pb isotope data calculated using the U concentrations estimated from the average Th/U ratio of the freshest samples (4.7 ± 0.7). A detailed documentation about how much this procedure affects the age correction of the measured isotope ratios is given in Appendices A and B.

4.3. Geochemical results

The freshest samples (LOI < 4.0 wt.%) have MgO values between 2.1 and 6.3 wt.%, except one sample (SO233 DR43-3) with 11.2 wt.% and SiO_2 contents from 47.6 to 51.6 wt.%. Our samples show a weak positive trend of MgO vs. CaO and negative trend of MgO vs. Al_2O_3 (Fig. A4 in Appendix A), pointing to clinopyroxene being a major fractionating phase. The large spread in FeO^* and TiO_2 values for samples with MgO < 4wt.% reflects variable degrees of Fe-Ti-oxide fractionation. In conclusion, irrespective of the LOI values, all samples lie within the compositional range of previously published lavas from the Tristan-Gough hotspot system (Fig. A4 in Appendix A).

Using the Nb/Y vs. Zr/Ti immobile element discrimination diagram (Pearce, 1996), the recovered lavas primarily plot in the basaltic field, however, nine plot within the alkali basalt and two samples (SO233 DR40-1 and DR19-1A) plot in the trachyandesite field (Fig. 2a). On a Nb/Yb vs. TiO_2/Yb plot (Fig. 2b), our samples show a crude positive slope extending from the tholeiitic EMORB and enriched tholeiitic OIB to the alkaline OIB field, consistent with lavas formed by a mantle plume interacting with a mid-ocean ridge (Pearce, 2008).

On incompatible multi-element diagrams (Fig. 3), all patterns have a pronounced negative Pb anomaly relative to the neighboring REEs (Ce and Pr, Nd), which is typical of oceanic basalts (OIBs and MORBs) (Fig. 3). All samples also show a negative Ti anomaly relative to Eu (Fig. 3). Overall the most incompatible elements are enriched relative to the less incompatible elements (Fig. 3). In general, the tholeiitic samples (Nb/Yb < 10, Nb/Y < 1; Fig. 2) have similar trace element patterns to previously published lavas from the Walvis Ridge (Fig. 3a; e.g., Gibson et al., 2005; Willbold and Stracke, 2006; Salters and Sachi-Kocher, 2010; Rohde et al., 2013a; Hoernle et al., 2015), whereas the alkali basalts (Nb/Yb > 10, Nb/Y > 1; Fig. 2) have comparable trace element patterns to lavas from the Guyot Province (including Gough island) with overall higher concentrations of the most incompatible elements, compared to tholeiitic samples with similar MgO contents (Fig. 3b).

Our new samples have the following isotope compositions characteristic of EMI-type lavas: radiogenic $^{87}Sr/^{86}Sr_{60Ma}$ (0.704–0.706), unradiogenic $^{143}Nd/^{144}Nd_{60Ma}$ (0.5123–0.5126) and $^{176}Hf/^{177}Hf_{60Ma}$ (0.2826–0.2828), and radiogenic $^{207}Pb/^{204}Pb_{60Ma}$ (15.46–15.63) and $^{208}Pb/^{204}Pb_{60Ma}$ (38.01–38.93) for a given $^{206}Pb/^{204}Pb_{60Ma}$ ratio (17.42–18.52)

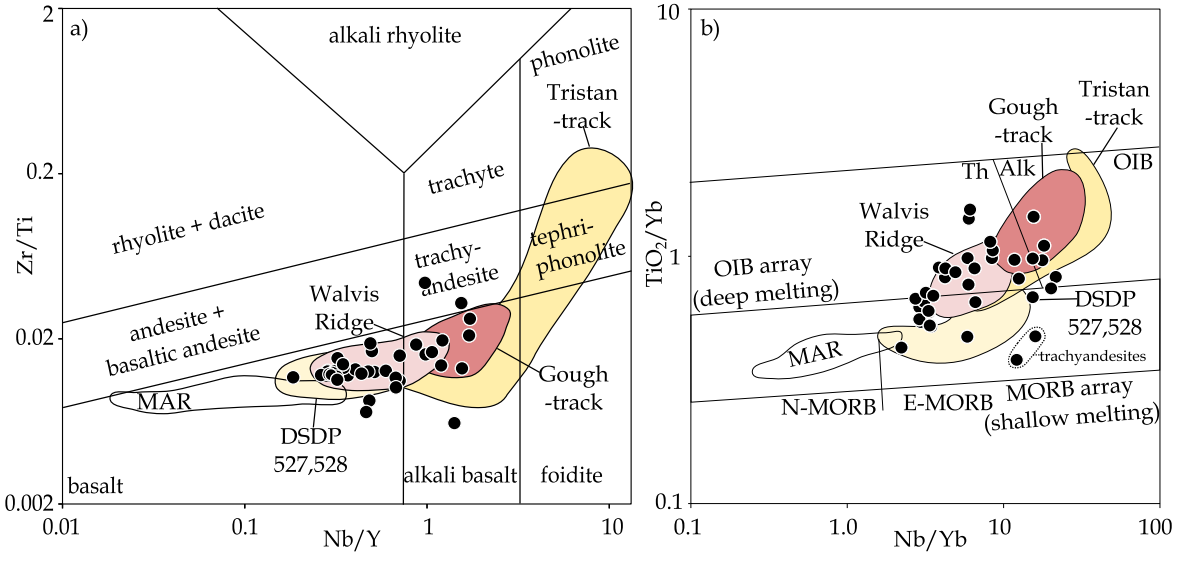

Fig. 2. Rock classification (a) Nb/Y vs. Zr/Ti plot using immobile trace element ratios and (b) Nb/Yb vsTiO_2/Yb after Pearce (1996) of the studied Walvis Ridge rocks compared to lavas from the Tristan-Gough hotspot track. The Tristan-type lavas are subdivided into Tristan sub-track in the Guyot Province (including Tristan islands) and DSDP Sites 527 & 528 on the Walvis Ridge, and the Gough-type lavas are divided into those from the Walvis Ridge (including DSDP Site 525) and the Gough sub-track in the Guyot Province (including Gough island). Also shown is the field for normal MAR basalts defined as having La/Yb ratios of <1 and La/Sm ratios of <1.5. Abbrevations: Th = tholeiites and Alk = alkaline. References for the literature data is reported in Fig. 1.

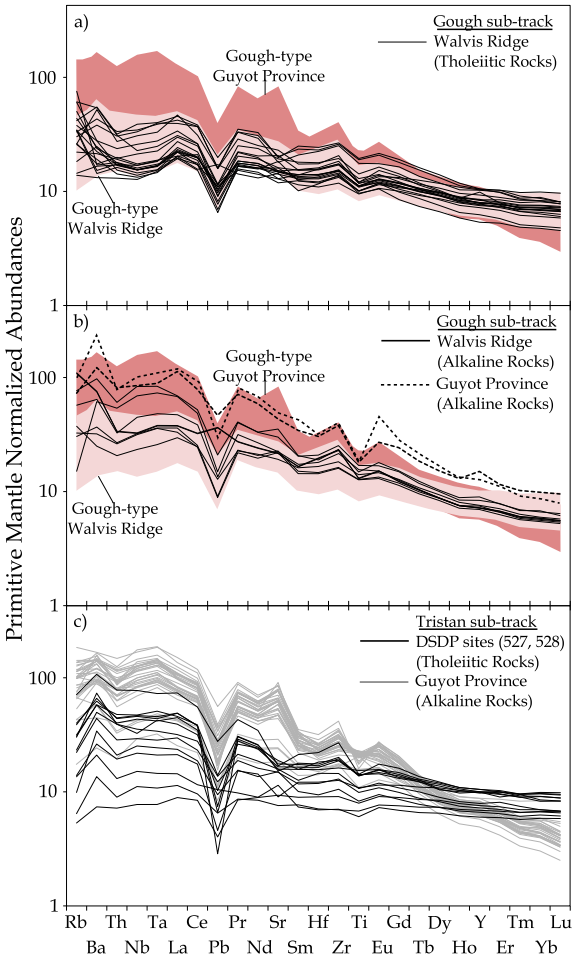

Fig. 3. Normalized incompatible element diagrams of (a) tholeiitic basement lavas from the Walvis Ridge, (b) alkaline lavas Gough-type lavas along the Tristan-Gough seamount chain compared to the Gough-type Guyot Province and Walvis Ridge lavas (including DSDP Site 525) from the literature (Fig. 1). (c) shows tholeiitic and alkaline lavas from DSDP Sites 527 & 528, Tristan sub-track Guyot Province (including Tristan da Cunha, Nightingale and Inaccessible) from the literature (see Fig. 1). The element concentrations are normalized to primitive mantle after Hofmann (1988). Only samples with MgO contents of >3 wt.% and LOI < 4 wt.% are shown.

(Fig. 4; Hart, 1984). In summary, the geochemical data lie largely within the range of previously published data for lavas from the Gough-type compositional group from the Tristan-Gough hotspot system (e.g., Gibson et al., 2005; Salters and Sachi-Kocher, 2010; Rohde et al., 2013a; Hoernle et al., 2015), but a few samples either expand the Gough-type field in multi-isotope space or have Tristan-type compositions (Fig. 4).

5. DISCUSSION

5.1. The age progressive Walvis Ridge

Previously $^{40}Ar/^{39}Ar$ ages from only five sample sites were available for the Walvis Ridge between the DSDP Sites and the northeastern end of the Walvis Ridge (Rohde et al., 2013b; O'Connor and Jokat, 2015a), which covers ~1500 km (nearly half) of the entire hotspot track. Of these five $^{40}Ar/^{39}Ar$ ages, only two were close to what was expected for a linear age progression, placing into question if the Walvis Ridge fits a simple age progressive hotspot model (Figs. 1 and 5). In an attempt to explain the lack of correlation in age versus distance, O'Connor and Jokat (2015a) invoked tectonic complexities related to plume-ridge interactions for the Walvis Ridge. Other models, proposed to explain the younger ages of some of the samples, include shallow tectonic processes (Fairhead and Wilson, 2005; Foulger, 2018). It should be noted, however, that the anomalously young lavas on the Walvis Ridge have distinct HIMU-type compositions (excluding sample AII93-21-1 with an EMI-type composition; Figs. 1, 5 and 6), indicating that the younger volcanism is not directly related to the Tristan-Gough hotspot (Homrighausen et al., 2018a, 2018b).

Our new $^{40}Ar/^{39}Ar$ data, together with previously published $^{40}Ar/^{39}Ar$ ages (Rohde et al., 2013b; O'Connor and Jokat, 2015a, 2015b), of samples with EMI-type composition (Figs. 4 and 6; excluding the aforementioned sample AII93-21-1) show a spatially continuous age progression along the entire Walvis Ridge beginning at 114.1 ± 0.4 Ma at the northeastern end, close to the Namibian coast (Rohde et al., 2013b), to 68.2 ± 0.7 Ma at DSDP Site 527 near the southeastern end (O'Connor and Jokat, 2015b). The $^{40}Ar/^{39}Ar$ age data of the EMI-type samples from the submarine Tristan-Gough hotspot track show an age progression of 31.05 mm/a ($R^2 = 0.97$; Fig. 5). The Etendeka flood basalts (135–132 Ma; Renne et al., 1996; Renne, 2015) and the Tristan da Cunha and Gough Islands (0.12–2.6 Ma; Maund et al., 1988; Hicks et al., 2012) plot close to this array, providing further support for the age progression (Fig. 5). Our calculated migration rate is significantly higher than the 26 mm/a proposed by O'Connor and Jokat (2015a), but is similar to the 30 mm/a rate proposed by Rohde et al. (2013b).

If the plate velocity has remained unchanged since ~115 Ma, as suggested by the data from the Tristan-Gough track (Fig. 5), then Tristan da Cunha and Gough Island may have already begun forming ~10 Ma ago. This implies that the inferred position of the hotspot(s) lie(s) ~310 km closer to the MAR than the presently active Tristan and Gough island complexes (Fig. 1). This is in good agreement with the presence of a low shear-wave-velocity anomaly in the upper mantle located ~200 km to the west of Tristan da Cunha rather than directly below it (Schlömer et al., 2017).

Most tholeiitic lavas along the entire Tristan-Gough hotspot track lie within ±4 Ma (2σ) of our calculated age progression line, whereas most alkaline lavas at the Walvis Ridge (e.g., sites SO233 DR41, SO234 DR4 & 6) show overall younger ages compared to the average age progression (see Appendix B). Late-stage (also referred to as rejuvenated or post-erosional) volcanism, occurring up to 15 Ma after the formation of the main volcanic edifice, is a characteristic feature of many intraplate volcanic systems, e.g., the Canary (≤15 Ma) and Hawaiian Islands (≤5Ma)

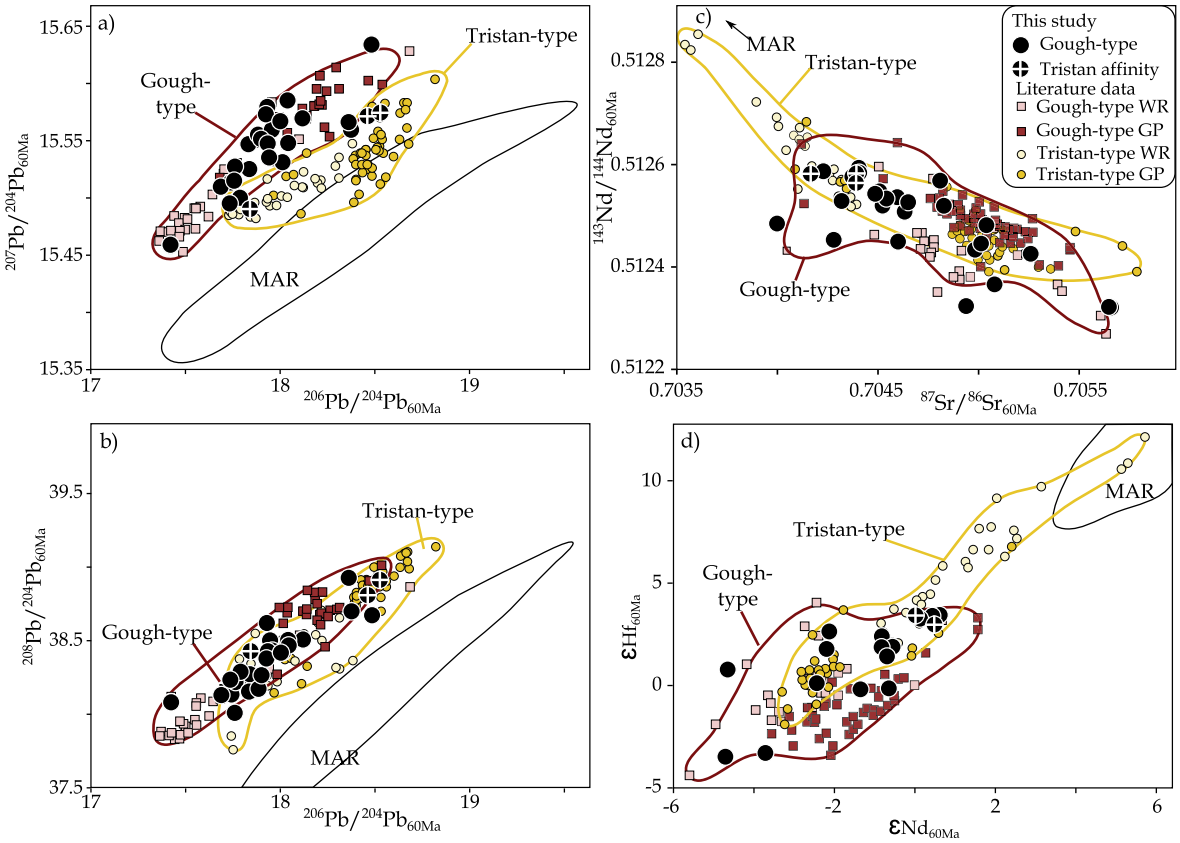

Fig. 4. Initial isotope ratios projected to 60 Ma using source parent/daughter ratios for the: (a) uranogenic ($^{206}Pb/^{204}Pb_{60Ma}$ vs. $^{207}Pb/^{204}Pb_{60Ma}$) and (b) thorogenic ($^{206}Pb/^{204}Pb_{60Ma}$ vs. $^{208}Pb/^{204}Pb_{60Ma}$) Pb isotope correlation diagrams, and (c) $^{87}Sr/^{86}Sr_{60Ma}$ vs. $^{143}Nd/^{144}Nd_{60Ma}$ and (d) εNd_{60Ma} vs. εHf_{60Ma} diagrams. The lavas from the Tristan-Gough hotspot track are divided into: (1) Gough-type composition, comprising lavas from the Walvis Ridge (including DSDP Site 525; Gough-type WR), Gough sub-track and Gough Island (Gough-type GP), and (2) Tristan-type composition, consisting of lavas from DSDP Site 527 & 528 on the Walvis Ridge (Tristan-type WR), Tristan sub-track and Tristan da Cunha Island (Tristan-type GP). For comparison, Mid-Atlantic Ridge (MAR) basalts with La/Yb < 1 and La/Sm < 1.5 are shown. Abbreviations: WR = Walvis Ridge and GP = Guyot Province.

(e.g. Hoernle and Schmincke, 1993; Garcia et al., 2010). Some lavas from the Walvis Ridge are up to 40 Ma younger than the age progressive EMI-type lavas (Rohde et al., 2013b; O'Connor and Jokat, 2015b; Homrighausen et al., 2018a), which is unusual for aseismic ridges and hotspot tracks. These "anomalously young" lavas were recovered from seamounts on or near the Walvis Ridge (Fig. 1; Homrighausen et al., 2018a, 2018b). Homrighausen et al. (2018a) showed that these lavas range in composition from St. Helena HIMU to EMORB-type compositions and conclude that these rocks were derived from a younger magmatic event unrelated to the Tristan-Gough mantle plume (Fig. 6). It was proposed that the younger lavas reflect mixing between a HIMU-type component derived from depth with shallow mantle (uppermost asthenosphere and lithosphere), reflecting interaction between the Tristan-Gough hotspot and the uppermost MORB source (DM) mantle (Homrighausen et al., 2018a).

In conclusion, the EMI-type Tristan-Gough hotspot track displays a well-constrained linear age progression (Fig. 5), consistent with an origin from a relatively stationary hotspot (mantle plume; e.g., Morgan, 1971; Wilson, 1973; Morgan, 1981; Campbell, 2007).

5.2. The Gough-type EMI composition: The dominant composition in South Atlantic hotspots

5.2.1. Emergence of the geochemical zonation in the Tristan-Gough hotspot track

The Tristan-Gough hotspot track comprises two EMI-type compositional fields that can be best distinguished using an uranogenic Pb isotope diagram, with Gough-type compositions having higher $^{207}Pb/^{204}Pb_{60Ma}$ at a given $^{206}Pb/^{204}Pb_{60Ma}$ ratio than Tristan-type EMI but with similar $^{208}Pb/^{204}Pb_{60Ma}$ ratios (Fig. 6). Most of our new samples lie within the Gough compositional domain, confirming that the Walvis Ridge consists primarily of the Gough-type EMI (Fig. 4). Nevertheless, a few samples either expand the Gough compositional field towards the Tristan field, or the first appearance of the Tristan-type EMI extends to about 90 Ma (Figs. 1, and 4). These lavas (SO234 DR6, SO233 DR16), however, were recovered from

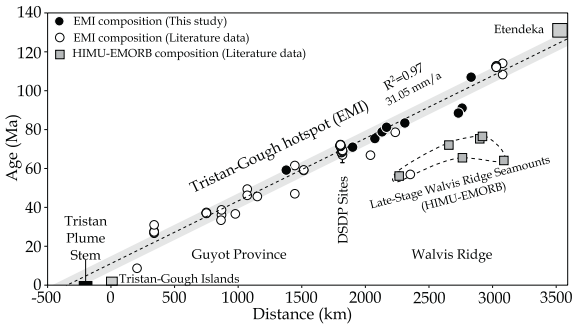

Fig. 5. Distance from the active volcanic islands (Tristan da Cunha and Gough) versus $^{40}Ar/^{39}Ar$ ages for samples from the Tristan-Gough hotspot track with EMI-type compositions (literature data = Rohde et al., 2013b; O'Connor and Jokat, 2015a, b). Sample sites were projected orthogonally to the proposed hotspot track (dashed line in Fig. 1). The dashed line in this figure shows the calculated age progression for the entire data set (31.05 mm/a; R^2 line fit = 0.96) of the submarine lavas for the Tristan-Gough hotspot track, excluding sample AII93-21-1. The grey field around the age progression line represents the duration of the main volcanic stage with an average age range of 8 Ma at a given location (i.e., distance from the islands), but this duration can be twice as long in some locations. The late-stage (post-erosional) volcanism, which is derived from seamount volcanoes on the eroded Walvis Ridge basement or adjacent to the ridge, has a distinct composition from the basement lavas (HIMU-EMORB versus EMI-type chemical composition) and is generally 20–40 Ma younger than the underlying basement at each location (Homrighausen et al., 2018a). The black bar marks the low velocity anomaly of the Tristian plume stem after Schlömer et al. (2017). The ages from Etendeka (135–132 Ma; Renne et al., 1996; Renne, 2015) and Tristan da Cunha and Gough islands (0.12–2.6 Ma; Maund et al., 1988; Hicks et al., 2012) are shown for comparison (large grey boxes).

the eastern side of the Walvis Ridge and thus the Tristan-track cannot be extended northward beyond the DSDP Sites on the Walvis Ridge, where the Tristan flavor occurs in the western DSDP Sites 527 and 528 (Fig. 1). No clear evidence has been found thus far for the presence of Tristan-type material during the formation of the Etendeka and Parana flood basalts (Hoernle et al., 2015). Only very limited data from two sites have been reported thus far from the Rio Grande Rise (Rohde et al., 2013a), which was located westward of the Walvis Ridge during its formation. It is not clear if these samples have Gough- or Tristan-type compositions, since they plot on the border of the two compositional fields, although Hoernle et al. (2015) interpreted them as Gough-type based on their Sr-Nd-Hf isotopic compositions. Another, thus far unsampled structure, is the Sao Paulo plateau, originally located north of the Florianopolis Fracture Zone and attached to the northernmost edge of the Walvis Ridge. Detailed sampling of both structures is needed to evaluate the history of geochemical zonation of the Tristan-Gough hotspot further back in time.

In conclusion, the Walvis Ridge is primarily characterized by a Gough-type composition, which reflects the dominant and long-lived EMI-type composition of the Tristan-Gough hotspot. The few possible Tristan-type lavas from the eastern side of the Walvis Ridge have comparable trace element concentrations and ratios (e.g., La/Sm = 5.2–6.5, La/Yb = 14.5–15.2 and Dy/Yb = 2.1–2.4) to nearby alkaline Gough-type lavas (i.e. SO233 DR19 and SO234 DR4; La/Sm = 4.9–8.4. La/Yb = 14.3–24.4 and Dy/Yb = 2.0–2.6). This suggests that the melting conditions (plume pudding model) were not the primary mechanism for generating the distinct isotopic signatures (Hofmann and Farnetani, 2013) and may also suggest limited local presence of Tristan-type material before the hotspot track became zoned (Fig. 1).

5.2.2. Origin of geochemical variations of the Gough-type EMI lavas

The vast majority of the Walvis Ridge lavas (including DSDP Site 525) have tholeiitic compositions, characterized by relatively low incompatible-element concentrations and low ratios of more to less incompatible elements (e.g., $Nb/Y < 1$, $Nb/Yb < 10$, $TiO_2/Yb < 1$, $Ti/V < 40$, $La/Sm < 4$, $La/Yb < 10$ for samples with MgO > 3wt.% and LOI < 5wt.%; Figs. 2 and 3). In contrast, the alkaline Gough-type lavas from the Guyot Province (including Gough Island) have relatively high incompatible-element abundances with higher more to less incompatible-element ratios ($Nb/Y > 1$, $Nb/Yb > 10$, $TiO_2/Yb > 1$, $Ti/V > 50$, $La/Sm > 4$, $La/Yb > 20$ for samples with MgO > 3wt.% and LOI < 5wt.%; Figs. 2 and 3). Overall, the differences between the tholeiitic and alkaline lavas reflect the change from plume-ridge interaction during the Walvis Ridge formation (e.g., Humphris and Thompson, 1983; O'Connor and Duncan, 1990), characterized by low-pressure and high-degrees (15–24%) of melting (Gibson et al., 2005; Salters and Sachi-Kocher, 2010), to intraplate volcanism during formation of the Guyot Province, characterized by an increase in lithospheric thickness resulting in higher pressures and lower degrees (5–8%) of melting (Gibson et al., 2005; Weit et al., 2017).

The Gough-type samples form a positive array on the uranogenic Pb isotope diagram (Fig. 4; $R^2 = 0.90$). The slope of this array is equivalent to an age of 2.4 Ga (Rohde et al., 2013a). Alternatively, this linear trend could be interpreted as a two-component mixing array of samples with unradiogenic and radiogenic Pb isotope ratios. The DSDP Site 525 lavas could serve as the unradiogenic end member (e.g., lower continental crust and/or subcontinental lithospheric mantle (SCLM); Zindler and Hart, 1986; Gibson et al., 2005; Salters and Sachi-Kocher, 2010; Rohde et al., 2013a). Considering all available isotope data, the Gough domain does not trend towards the FOZO/PREMA or EMII end member compositions (Fig. 4). FOZO/PREMA-type melts (e.g., Comoros), mixed with a small proportion of melts with EMII-type composition (~10% EMII-type lavas from the Kerguelen plateau; Ingle et al., 2002), could form a suitable end member with radiogenic Pb (Fig. 6). In this case, mixing of recycled lower continental crust or SCLM having an EMI-type composition (e.g., Gibson et al., 2005; Rohde et al., 2013a; Hoernle et al., 2015) with a mixture of recycled oceanic crust having a FOZO/PREMA-type composition (e.g.

Stracke et al., 2005; Stracke, 2012) and marine sediments or upper continental crust having an EMII-type composition (Fig. 6) could reproduce the Gough arrays on Sr-Nd-Pb-Hf isotope diagrams.

5.2.3. A common EMI-type in South Atlantic hotspots

The Discovery seamount chain also represents a long-lived (~40 Ma) spatially-zoned hotspot track in the South Atlantic (Fig. 1; Schwindrofska et al., 2016). The Northern Discovery seamounts have compositions lying within the Gough-type EMI domain on Sr-Nd-Pb-Hf isotope plots, suggesting derivation from a common Gough source (Fig. 6; Schwindrofska et al., 2016).

The isotopic composition of the lavas from the Shona hotspot track largely overlap with the Gough-type lavas from the Tristan-Gough track in isotopic composition, but many samples trend to lower $^{207}Pb/^{204}Pb_{60Ma}$, $^{208}Pb/^{204}Pb_{60Ma}$ and $^{87}Sr/^{86}Sr_{60Ma}$ ratios, but higher $^{143}Nd/^{144}Nd_{60Ma}$ and $^{176}Hf/^{177}Hf_{60Ma}$ ratios at given $^{206}Pb/^{204}Pb_{60Ma}$ ratios (Fig. 6). In contrast to the Tristan-type composition, the range of Shona isotopic compositions is consistent with mixing of Gough-type EMI and a depleted MORB-like component (Fig. 6; Hoernle et al., 2015, 2016).

In conclusion, the Gough-type composition can be identified in the Tristan-Gough, Discovery and Shona hotspot tracks and thus represents the most widespread EM-type in the South Atlantic. The common and long-term (up to ~135 Ma) presence of this component in the South Atlantic hotspot tracks suggests that this EMI-type mantle plume material is derived from a common reservoir (Class and le Roex, 2011; Hoernle et al., 2016; Schwindrofska et al., 2016).

5.2.4. Deep or shallow origin of the widespread Gough-type EMI composition?

Overall, the excellent age progressions along the entire Tristan-Gough (Fig. 5), Discovery (Schwindrofska et al., 2016) and Shona (O'Connor et al., 2012; Hoernle et al., 2016) hotspot tracks indicate relatively stationary melt anomalies in the uppermost mantle (Figs. 1 and 5). The continuous presence of the Gough-type EMI signature over ~135 Ma along the Tristan-Gough, ~40 Ma along the Discovery, and >84 Ma along the Shona hotspot tracks

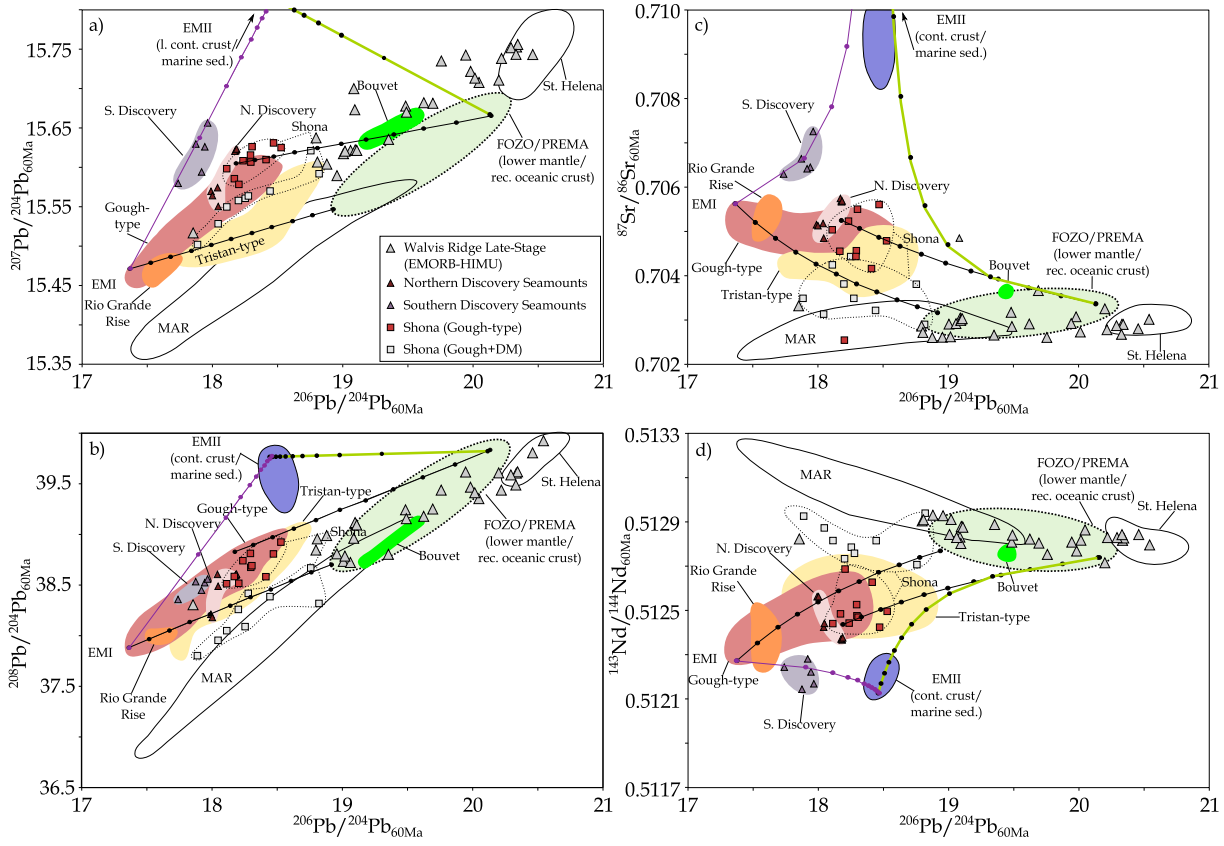

Fig. 6. Initial isotope ratios projected to 60 Ma for South Atlantic intraplate lavas on $^{206}Pb/^{204}Pb_{60Ma}$ ratios vs. (a) $^{207}Pb/^{204}Pb_{60Ma}$, (b) $^{208}Pb/^{204}Pb_{60Ma}$, (c) $^{87}Sr/^{86}Sr_{60Ma}$, and (d) $^{143}Nd/^{144}Nd_{60Ma}$ ratios. The diagrams show that the Shona and Northern Discovery lavas lie within the Gough-type compositional array. Mixing lines between: (1) Gough-type and FOZO/PREMA (Comoros; black lines), (2) FOZO/PREMA and EMII (Elan bank sediments; green line) and (3) Gough-type and EM II (purple line) are shown. The compositions of the mixing components are reported in Appendix A. Abbreviations: l. cont. crust = lower continental crust, sed. = sediment, rec. oceanic crust = recycled oceanic crust, and cont. crust = continental crust. (For interpretation of the references to colour in this figure legend, the reader is referred to the web version of this article.)

(possibly up to 180 Ma, if the Karoo flood basalts are part of the Shona track; Torsvik et al., 2006, 2010) points to a continuous supply of such material to these mantle plumes from a large-scale reservoir.

Along the entire South Atlantic MAR, EMI-type flavors have only been reported from ridge segments close to the proposed hotspots consistent with plume-ridge interaction (Schilling et al., 1994; Fontignie and Schilling, 1996; Douglass et al., 1999; Le Roux et al., 2002). Other parts of the southern MAR also have "enriched" geochemical characteristics that are not characteristic of a depleted upper mantle normal MORB source. These MAR segments have high $^{206}Pb/^{204}Pb$ and $^{87}Sr/^{86}Sr$ and low $^{143}Nd/^{144}Nd$ ratios and low Nb concentrations with high Ba/Nb, La/Nb and K/Nb ratios, but are clearly unlike EMI or EMII type material (e.g. Escrig et al., 2005). Le Roux et al. (2002) proposed that this signature in some MAR segments is related to low-volume asthenospheric contamination inherited from long-lasting subduction zones (Devonian to Mesozoic) along the south-southwestern Gondwana margin. Since EMI material is absent along the South Atlantic MAR away from the hotspots, a deep origin of the EMI Gough-type composition follows (Richardson et al., 1982; Hanan et al., 1986; Weaver et al., 1987; Fontignie and Schilling, 1996; Le Roex et al., 2010; Class and le Roex, 2011; Rohde et al., 2013a, 2013b; Hoernle et al., 2015, 2016; Schwindrofska et al., 2016).

Further hints for a deep origin of this EMI-type mantle comes from seismic tomography, which images a low-velocity, conduit-like structure with a radius of ~200 km to a possible depth of ~500 km, located southwest of Tristan da Cunha (Schlömer et al., 2017). This shallow velocity anomaly overlies a broad (800–1000 km) vertically continuous dome-like structure with ∂V_s ratios of $<-0.5\%$ in the depth range of 1000–2800 km (French and Romanowicz, 2015). The Discovery hotspot seems to overlie the same broad velocity anomaly as the Tristan-Gough mantle plume in the lowermost mantle (see seismic tomographic cross-sections in the extended data Fig. 2f–j in French and Romanowicz, 2015), consistent with a common lower mantle upwelling, which splits in the uppermost 1000 km of the mantle into several distinct mantle plumes (also referred to as secondary mantle plumes; Courtillot et al., 2003; Suetsugu et al., 2009; French and Romanowicz, 2014). Due to the small diameter of the secondary plumes, they are often below the resolution that can be detected in whole-mantle seismic models (e.g., French and Romanowicz, 2015). A similar broad, but less continuous structure is observed in the lower mantle beneath the Shona and Bouvet hotspots (Zhao, 2007; French and Romanowicz, 2015), and a smaller shear wave anomaly in the upper mantle beneath the Bouvet hotspot (Montelli et al. (2006). In summary, seismic low-velocity anomalies suggest broad mantle upwellings in the lower mantle that form dome-like structures to depths of ~1000 km, whereas at depths above ~1000 km several distinct secondary mantle plumes form that rise beneath the Tristan-Gough, Discovery, Shona and Bouvet hotspots (Montelli et al., 2006; Zhao, 2007; French and Romanowicz, 2015; Schlömer et al., 2017).

Additional evidence for a lower mantle origin of the Gough-type EMI mantle comes from primitive noble gas isotopes. Stroncik et al. (2017) found high $^3He/^4He$ ratios of up to 26 R_A in three out of 14 samples from dikes of the Etendeka flood basalt province, demonstrating that the Tristan-Gough mantle plume incorporated Gough-type material from the lower mantle during its initial stage. On the other hand, a few samples from Tristan da Cunha and Gough (two from each island) display low $^3He/^4He$ ratios (<6.3 R_A; Kurz et al., 1982). Studies from Etendeka and Hawaii show that low helium ratios in some lavas coexist with primitive noble gas signatures in other lavas from the same volcanic province or even volcano (Kurz et al., 2004; Stroncik et al., 2017). Stroncik et al. (2017) argued that most Etendeka dikes had degassed their primitive He and were crustally contaminated and pointed out that high $^3He/^4He$ ratios are rare. At Hawaii, the $^3He/^4He$ ratios in the Hawaiian Scientific Drilling Project (HSDP) core overall increase with increasing depth from MORB-type ratios (some are lower than 8 R_A) to ~12-14R_A and up to 25R_A at depth within the core (Kurz et al., 2004), although the trace elements and Sr-Nd-Pb-Hf isotope signatures of the lavas with low He isotope ratios remain characteristic of the Hawaiian plume (Blichert-Toft et al., 2003; Eisele et al., 2003; Rhodes and Vollinger, 2004; Bryce et al., 2005). Overall, the primitive He isotope signature appears to decline during later stages of ocean island volcanism, when the volcano is no longer directly above the center of the hotspot (e.g., Bryce et al., 2005). The offset of the Gough and Tristan island/seamount groups from the spatial age progression defined by the submarine lavas (Fig. 5), together with the location of the seismic low-velocity anomaly SW of Tristan (Schlömer et al., 2017), indicate that at least Tristan da Cunha does not overlie the center of the present mantle upwelling. The young surface lavas (e.g., ankaramitic basanites) used for the noble gas study of Kurz et al. (1982) most likely represent post-shield (or even rejuvenated) volcanism and thus degassed plume material from the margins of the plume, which is the same as observed during the post-shield volcanism in Hawaii. Therefore, the low helium isotope ratios from the four probable post-shield-stage lavas do not necessarily exclude a primitive mantle signature for the Tristan-Gough mantle plume. Finally, the high $^3He/^4He$ isotope ratios (up to 15 R_A) and other primitive noble gas isotope signatures in basalts from the MAR segments adjacent to the Northern Discovery and Shona hotspots provide evidence that present-day Gough-type EMI still contains a primitive gas signature from the lowermost mantle (Douglass et al., 1999; Sarda et al., 2000; Schwindrofska et al., 2016).

In summary, the combination of: (1) a systematic age progression (pointing to a relatively stationary long-term melt anomaly), (2) a constant Gough-type EMI composition over 135 Ma, (3) primitive noble gas signatures in some plume-related Gough-type EMI lavas in the initial Tristan-Gough stage and in present-day Discovery and Shona lavas erupted at the MAR (indicating that this material is derived from the lower mantle), and (4) low-velocity anomalies beneath the South Atlantic EMI-type hotspots that extend

to the base of the lower mantle (consistent with upwelling of mantle from the base of the lower mantle at the margin of the African LLSVP) provide strong evidence for the origin of the Gough-type plume material in the Tristan-Gough, Discovery and Shona hotspots from a common reservoir in the lower mantle.

5.3. Geochemical heterogeneity in the South Atlantic

5.3.1. The origin of the Tristan and Southern Discovery EMI-type flavors

In general, the distinct compositional fields in the southern South Atlantic Ocean form a crude array in $^{206}Pb/^{204}Pb_{60Ma}$ versus $^{208}Pb/^{204}Pb_{60Ma}$, $^{87}Sr/^{86}Sr_{60Ma}$, $^{143}Nd/^{144}Nd_{60Ma}$, and $^{176}Hf/^{177}Hf_{60Ma}$ isotope correlation diagrams (Fig. 6; see also Fig. 6 in Schwindrofska et al. (2016)). It has been proposed that the compositional range could have formed by mixing of two principal types of components (Geldmacher et al., 2008; Schwindrofska et al., 2016): (a) a range of EMI-type low-μ components (with highly variable $^{207}Pb/^{204}Pb$, but relatively constant low $^{206}Pb/^{204}Pb$, intermediate $^{208}Pb/^{204}Pb$ and high Sr, but low Nd and Hf isotope ratios) and (b) a component with higher $^{206}Pb/^{204}Pb$, such as FOZO/PREMA and/or HIMU ± DM (depleted mantle) (with high $^{207}Pb/^{204}Pb$ and $^{208}Pb/^{204}Pb$ and intermediate Sr, Nd and Hf isotope ratios). The low-μ component could have been formed by variable but low time-integrated U/Pb ratios and/or different reservoir formation ages (see Geldmacher et al., 2008, for detailed discussion). Alternatively, Stracke (2012) proposed a three step mixing scenario to explain the continuous arrays of EM-type OIBs: (1) a mixture of EMI and EMII resulting in EM, (2) a mixture of EM with FOZO/PREMA, and (3) variable dilution of the EM-FOZO/PREMA mixture with DM.

The composition of the Tristan-type compared to the Gough-type component could be explained by mixing with a FOZO/PREMA-like component (Gibson et al., 2005; Salters and Sachi-Kocher, 2010). Mixing of FOZO/PREMA-like melts (such as Comoros lavas) with Gough-type melts could generate the Tristan compositional range on a thorogenic Pb diagram, but would displace it to distinctly lower $^{207}Pb/^{206}Pb$ ratios on the uranogenic Pb isotope diagram (Fig. 6). In contrast, mixing of St. Helena HIMU and Gough-type EMI melts requires additional dilution by DM to reproduce the Tristan-type EMI on the uranogenic Pb isotope diagram, which is inconsistent with the thorogenic isotope diagram (Fig. 6). Therefore, we propose the prevalent FOZO/PREMA-like composition as a potential mixing component, which was also proposed by Salters and Sachi-Kocher (2010) for the DSDP Site 527 and 528 lavas.

The Southern Discovery seamounts have higher $^{207}Pb/^{204}Pb_{60Ma}$ and $^{87}Sr/^{86}Sr_{60Ma}$ ratios, and lower $^{143}Nd/^{144}Nd_{60Ma}$ and $^{176}Hf/^{177}Hf_{60Ma}$ ratios, but similar $^{208}Pb/^{204}Pb_{60Ma}$ ratios at a given $^{206}Pb/^{204}Pb_{60Ma}$ ratio compared to Gough (Fig. 6). This composition represents the third distinct and the most enriched EMI-type composition in the South Atlantic. Mixing of small proportions of EMII-like upper continental crustal melts with DSDP Site 525 Gough-type EMI (characterized by low $^{206}Pb/^{204}Pb$) could reproduce the Southern Discovery isotopic signature (Fig. 6).

In summary, the geochemical heterogeneities in the South Atlantic DUPAL anomaly can be explained by a common DSDP Site 525 Gough-type EMI composition, which mixes with different proportions of FOZO/PREMA and EMII. Since the Gough-type composition can be reproduced by mixing of recycled lower continental crust or SCLM (EMI, e.g., Gibson et al., 2005; Rohde et al., 2013a; Hoernle et al., 2015) with recycled oceanic crust (FOZO/PREMA; Stracke et al., 2005; Stracke, 2012 and references therein) and sediments (EMII), the entire South Atlantic DUPAL-anomaly could be formed by variable mixing proportions of these three components (Fig. 6).

5.3.2. FOZO/PREMA and HIMU in the South Atlantic

Apart from the Gough, Tristan and Southern Discovery EMI-type compositions, Bouvet Island, the southernmost proposed mantle plume in the South Atlantic (Le Roex et al., 1985; Kurz et al., 1998; Douglass et al., 1999; Montelli et al., 2006), is characterized by intermediate Pb, Sr and Nd isotope ratios and has a FOZO/PREMA-like composition (Fig. 6). Mid-ocean ridge (MOR) lavas adjacent to Bouvet Island, which show the influence of the Bouvet plume in their Sr-Nd-Pb isotope composition, have high $^{3}He/^{4}He$ isotope ratios of up to 14 R_A, indicating the presence of primitive material from the lower mantle (Kurz et al., 1998). Bouvet Island overlies a seismic low-velocity anomaly that extends into the lower mantle, providing further evidence for a lower mantle origin of the FOZO/PREMA composition (Montelli et al., 2006; Zhao, 2007; French and Romanowicz, 2015).

In addition to the EMI and FOZO/PREMA components, a distinct type of intraplate lava (with radiogenic Pb and intermediate Sr-Nd-Hf isotope ratios, referred to as HIMU) characterizes the South Atlantic ocean basin. St. Helena Island represents the South Atlantic type locality for the HIMU end member (e.g., Zindler and Hart, 1986). Late-stage lavas with St. Helena HIMU end member compositions have been reported from the Walvis Ridge and Shona (Richardson seamount) hotspot tracks (Fig. 1; Homrighausen et al., 2018a; Homrighausen et al., 2018b). Lavas with a St. Helena HIMU composition and similar ages to the late-stage Shona and Tristan-Gough lavas are also reported from the West African coast (Cooper and Reid, 1998; Cooper and Reid, 2000; Davies et al., 2001; Janney et al., 2002; Luchs et al., 2013), indicating that they were part of a larger-scale event (Homrighausen et al., 2018a). Since there is no evidence that HIMU is stored in the African SCLM (see Janney et al. (2002) and Homrighausen et al. (2018a) for detailed discussions) and seismic tomography images a conduit-like structure from the upper to the lowermost mantle beneath St. Helena (e.g., Montelli et al., 2006; French and Romanowicz, 2015), it seems most likely that St. Helena HIMU is also derived from the lowermost mantle. In this case, the HIMU material observed in the entire South Atlantic realm is most likely derived from the lower mantle in the form of weak mantle plumes or blobs (Homrighausen et al., 2018a).

6. WHAT IS THE ORIGIN OF CHEMICAL HETEROGENEITIES IN SOUTH ATLANTIC HOTSPOTS?

We now summarize the geochemical heterogeneity of the South Atlantic hotspot volcanism in order to evaluate source heterogeneities. We will begin with the EMI-type hotspots. Several observations provide strong evidence that the Tristan-Gough, Discovery and Shona hotspot tracks are formed by mantle plumes that sample a common Gough-type EMI reservoir at the base of the lower mantle (Section 5.2.4). Numerous studies have pointed out the association of plumes with the margins of the African and Pacific Large Low-Shear Wave Velocity Provinces (LLSVPs), suggesting that plumes are preferentially generated/anchored along the Pacific and African LLSVP margins with the margin of the LLSVP serving as a guide for deflecting mantle flow upwards to form plumes (e.g. Thorne et al., 2004; Torsvik et al., 2006; Burke et al., 2008; Garnero and McNamara, 2008; Steinberger and Torsvik, 2012; French and Romanowicz, 2015). Considering that all three hotspots with the common Gough-type signature (Section 5.2.3; Fig. 6) are located above the margin of the African LLSVP (Fig. 1), their common source reservoir could either be located within the LLSVP (or ultra-low-velocity zones at the margins of the LLSVP; McNamara et al., 2010) or represent the ambient mantle outside the LLSVP.

Similar to hotspot tracks in the Pacific, such as the Galapagos (e.g. Hoernle et al., 2000; Harpp and White, 2001; Werner et al., 2003) and Hawaii (Abouchami et al., 2005; Huang et al., 2011; Weis et al., 2011), the Tristan-Gough and the Discovery hotspots show spatial geochemical zonation that can be traced back to at least ~70 Ma and ~40 Ma respectively (Section 5.2.1). Since several zoned hotspot tracks are associated with the margins of the LLSVPs, most recent studies assign the source of the more enriched material to the main body of the LLSVP (e.g. Loa- or Gough-type) and the less enriched component to ambient mantle entrained from outside of the LLSVP (e.g. Kea- or Tristan-type) (e.g., Huang et al., 2011; Weis et al., 2011; Rohde et al., 2013a; Harpp et al., 2014; Hoernle et al., 2015; Schwindrofska et al., 2016; Harrison et al., 2017). Tank experiments and numerical models on purely thermal mantle plumes show that spatial heterogeneities in the basal thermal boundary layer can be preserved through laminar flow in the rising plume (e.g., Kerr and Mériaux, 2004; Farnetani and Hofmann, 2009; Lohmann et al., 2009; Farnetani et al., 2012; Hofmann and Farnetani, 2013). The LLSVPs, however, most likely have a thermochemical origin (i.e. are denser and hotter compared to the ambient mantle; e.g., Garnero and McNamara, 2008; Ballmer et al., 2016 and references therein). Numerical simulation of thermochemical mantle plumes show that if the respective sources producing the zonation exhibit physical contrasts (i.e. density), as would be expected if plumes tapped both the LLSVP and surrounding mantle, then the plumes should be concentrically zoned with the denser material (in this case from the LLSVP) being drawn into the center of the plume (Jones et al., 2016). A concentric plume arriving at the base of the lithosphere, however, would not generate a bilaterally zoned hotspot track. Therefore, either zoned plumes don't tap reservoirs with distinct densities or there must be an additional mechanism to produce bilaterally asymmetrical plume and hotspot track zonation.

As an alternative to the laterally zoned plume model, a heterogeneous "plume pudding" model has been proposed to explain lateral zonation in hotspot tracks (Bianco et al., 2008, 2011; Ballmer et al., 2011; Jones et al., 2017). This model invokes a plume consisting of a uniform mixture of one or more enriched and fertile recycled components (e.g., eclogite/pyroxenite) within a more depleted and refractory plume matrix (e.g., peridotite), whereby shallow processes such as variations in lithospheric thickness (depth of melting) lead to compositionally distinct melting trends. With respect to the Tristan-Gough hotspot track, it has been argued that such a model is inconsistent with several geochemical observations (Hoernle et al., 2015). For example, the Gough-type EMI is the dominant composition during the formation of Walvis Ridge through plume-ridge interaction, where melting was shallower and the degree of melting was higher compared to the Guyot Province (see Section 5.2.2). In accordance with the plume pudding model, the Gough-type composition would then represent the low-pressure, high-degree melt of the depleted plume matrix, whereas the Tristan-type EMI composition would represent the high-pressure, low-degree melt from fertile eclogite/pyroxenite. Therefore, we would expect a transition from Gough- to Tristan-type composition with decreasing age coupled with the transition from plume-ridge to an intraplate setting. The geochemical zonation, however, starts at ~70 Ma (Section 5.2.1) shortly before the transition of the geodynamic setting (Section 5.2.3). The Tristan-track lies on 10–30 Myr younger and thus thinner oceanic lithosphere relative to the Gough-track, and thus should be derived from the more refractory Gough component (Hoernle et al., 2015). Changes in melt composition, reflecting a change in the proportion of fertile to refractory components contributing to the melts, should also be observed when a fracture zone, serving as a boundary between different aged lithosphere with different thicknesses, passes over the hotspot. Such changes, however, are not observed when the Tristan-Gough and Discovery hotspot tracks cross fracture zones. We therefore conclude that the plume pudding model cannot easily explain the geochemical observations in the South Atlantic and thus favor a laterally zoned plume model.

Seismic models can provide additional constraints on the nature of plume upwelling. They indicate a broad lower-mantle, cylindrical or dome-like upwelling, which tops out at a depth of ~1000 km (French and Romanowicz, 2015). At shallower depths (above 500 km) smaller conduit-like structures can be distinguished (Zhao, 2007; Schlömer et al., 2017; see Section 5.2.4), consistent with secondary plumes rising from the top of the larger dome-like upwelling (Courtillot et al., 2003). As discussed above, Tristan and Southern Discovery compositions can be generated by mixing variable proportions of the Gough composition with variable mixtures of FOZO/

PREMA (recycled ocean crust; e.g., Stracke et al., 2005; Stracke, 2012 and references therein) and EMII (recycled marine sediments, e.g. Zindler and Hart, 1986) (see Section 5.3.1). Interestingly, the Gough-type tracks (Walvis Ridge and Gough sub-track, and Northern Discovery Seamounts) overlie the central portions of this broad lower mantle upwelling, whereas the Tristan-type and Southern Discovery Seamount lavas are located closer to its margins (Fig. 7). The observed geochemical pattern, projected down to the top of the broad velocity anomaly (~1000 km), could reflect a concentric mantle plume (Jones et al., 2016) that taps denser Gough-type EMI material derived from the LLSVP, carried on the central portion of the mantle upwelling, and heterogeneous ambient mantle from outside of the LLSVP, carried in the outer portions of the upwelling (Fig. 7). In this case, the ambient mantle outside the LLSVP could represent heterogeneous domains, which are dominated by EMII or FOZO/PREMA (Fig. 7). In this model, the secondary mantle plumes from the central portion of the broad dome-like structure are dominated by Gough-type composition (Walvis Ridge and Gough sub-track, and Northern Discovery Seamounts), whereas the marginal secondary plumes represent mixtures of Gough-type and the outer portions (FOZO/PREMA or EMII) of the broader/deeper mantle upwelling (Fig. 7). Accordingly, the broad lower mantle upwelling beneath the Shona and Bouvet hotspots could also reflect a concentric plume with Gough-type material in the central portions surrounded by FOZO/PREMA-type lithologies, which feeds two distinct secondary plumes in the upper mantle.

The location and geochemical arrangement of the South Atlantic plumes is consistent with the model for plume generation zones at the margins of the LLSVPs (Burke et al., 2008), specifically that "graveyards" of subducted material lie outside of the LLSVPs (e.g., Burke et al., 2008; Garnero and McNamara, 2008; Wang et al., 2013; Li et al., 2014). Subducting slabs may even serve as push brooms to drive heated (from the core), older subducted materials against the LLSVP boundaries, generating upwellings (mantle plumes) that sample subducted material from outside the

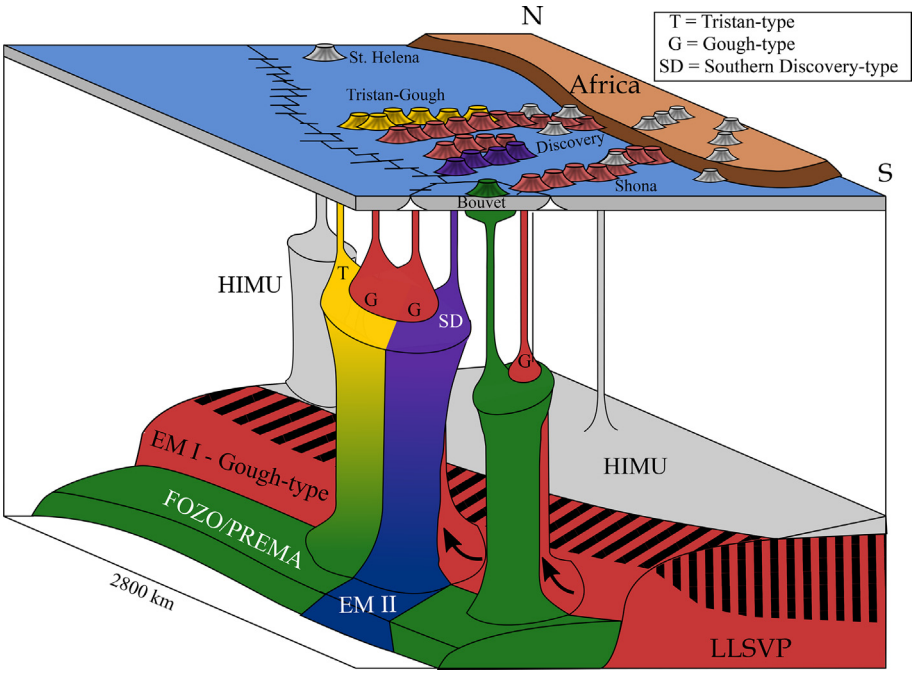

Fig. 7. A possible model to explain the observed geochemical and seismic variations and numerical simulations related to the origin of the South Atlantic intraplate magmatism. Following the seismic tomographic model of French and Romanowicz (2015) the Tristan-Gough and Discovery mantle plumes rise from the same broad velocity anomaly extending from 1000–2800 km depth in the lower mantle, which ultimately rises from the margin of the African LLSVP. This broad anomaly splits into several distinct secondary mantle plumes in the upper mantle (French and Romanowicz, 2015; Schlömer et al., 2017). We propose that the Gough-type composition (G; red) forms the margin of the African LLSVP and the HIMU-type composition (grey) is located in a more internal portion of the African LLSVP. In accordance with the numerical simulations of Jones et al. (2016), the more dense Gough-type material is drawn into the center of the upwelling mantle, whereas the ambient mantle outside the LLSVP surrounds it. Subducting oceanic lithosphere (green, FOZO/PREMA; Stracke, 2012), eroded continental crust and/or pelagic sediments (blue, EMII), could push mantle material up against the margins of the LLSVP triggering mantle upwellings (Burke et al., 2008). Therefore, the Tristan-type composition (T; yellow) could represent entrainment and mixing of Gough EMI- and FOZO/PREMA-type materials, whereas the Southern Discovery-type composition (SD: purple) could be generated by entrainment and mixing of Gough-type mantle (EMI) with EMII-like mantle. The mixing could take place at the margin of the LLSVP, during mantle plume ascent or at the transitional zone. HIMU volcanism on the Walvis Ridge, Shona hotspot track and West Africa could be derived from weak secondary mantle plumes/blobs between 70 and 50 Ma (Janney et al., 2002; Homrighausen et al., 2018a). (For interpretation of the references to colour in this figure legend, the reader is referred to the web version of this article.)

LLSVPs and material from the LLSVP rims. We note that although this represents our favored scenario, which is consistent with the present geochemical and seismic data, this is not a unique explanation. For example, it is also possible that all the different geochemical flavors originate outside of the LLSVP (representing a graveyard for subducted ocean lithosphere, continental material removed by subduction erosion and delaminated SCLM and lower continental crust) and that no LLSVP material is sampled. This could explain why the boundaries between the different geochemical zones in many zoned hotspot tracks/plumes are not oriented parallel to the margins of the LLSVP but rather orthogonal to them (Rohde et al., 2013a; Schwindrofska et al., 2016). Finally, it also cannot be ruled out that some material (e.g. Tristan, Southern Discovery and/or Bouvet) is picked up at mid-mantle depths, for example above the large dome-like upwellings.

Finally we address the origin of the HIMU-type lavas from (1) St. Helena, (2) late-stage Tristan-Gough and Shona, and (3) western Africa, which are also likely to be derived from the lower mantle (see Section 5.3.2). In contrast to the lavas derived by plumes lying above the margin of the African LLSVP, all of these HIMU-type lavas were erupted when the lithosphere beneath them was located over internal portions of the African LLSVP (Fig. 1; Homrighausen et al., 2018a). Seismic tomography shows that the St. Helena plume can be traced to the top of the African LLSVP, not to its margin (French and Romanowicz, 2015; Fig. 3d). The St. Helena HIMU-type lavas, superimposed on the Tristan-Gough and Shona tracks, were emplaced ~20–50 Ma after the cessation of EMI-type volcanism, corresponding to a distance of 600–1500 km between contemporaneous EMI and HIMU type volcanism, using an average African plate velocity of ~ 30 mm/a (Fig. 5). Since the EMI-type basement lavas of the Tristan-Gough, Discovery and Shona hotspot tracks show no evidence of St. Helena HIMU material, the HIMU source reservoir is most likely spatially isolated from the EMI source reservoir. This observation suggests that either the internal portions of the African LLSVP contain HIMU or alternatively that HIMU-type mantle is stored on top of the internal portions of the LLSVP (Fig. 7; Homrighausen et al., 2018a). The observation that EMI-type hotspots are derived from plumes associated with the margin of the African LLSVP and that the HIMU-type upwellings are located above interior portions of the LLSVP could reflect compositional layering within the LLSVP (Ballmer et al., 2016 and references therein). The layered LLSVP model predicts that long-lived "primary" plumes rise from the LLSVP margins and tap the lower compositional layer (Ballmer et al., 2016). These "primary" plumes can entrain a mixture of material including primordial mantle (Ballmer et al., 2016), consistent with the primitive noble gas signature of the Tristan-Gough, Discovery, Shona and Bouvet plumes. The model also predicts that short-lived "secondary" plumes will rise from the roofs of the LLSVPs, tapping a distinct higher level, possibly basaltic, reservoir in the upper part of the LLSVPs (Ballmer et al., 2016). This could be the source of the weaker, short-lived HIMU-type volcanism.

In conclusion, although the above considerations are highly speculative, as is any discussion of the geochemical heterogeneity of the lower mantle, we have tried to combine spatial and temporal geochemical variations of hotspots with seismic tomography and dynamic modelling in order to explain the origin of South Atlantic/West African intraplate volcanic rocks and lower mantle geochemical heterogeneity. Although our model is not unique, it is consistent with the available constraints and hopefully will provide a framework for future studies of geochemical variations within intraplate volcanism.

ACKNOWLEDGMENTS

We thank Captain Meyer and the crew of the R/V SONNE for their support during cruises SO233-Walvis II and SO234/1-Spaces; S. Hauff, K. Junge, J. Sticklus and U. Westernströer for analytical support; and M. Anders for help with sample preparation. We further thank A. Stracke, B. White, E. Brown and S. Gibson for constructive reviews that helped improve this manuscript. This study and Ph.D. position of S.H. were funded by the German Ministry for Research and Education (BMBF; grants SO233-Walvis II to KH and FH and SO234/1-Spaces to RW) and the GEOMAR Helmholtz Center for Ocean Research Kiel.

DECLARATION OF INTEREST

Conflicts of interest: None.

APPENDIX A. SUPPLEMENTARY MATERIAL

Supplementary data to this article can be found online at https://doi.org/10.1016/j.gca.2018.09.002.

REFERENCES

Abouchami W., Hofmann A., Galer S., Frey F., Eisele J. and Feigenson M. (2005) Lead isotopes reveal bilateral asymmetry and vertical continuity in the Hawaiian mantle plume. *Nature* **434**, 851.

Baksi A. K. (2007) A quantitative tool for detecting alteration in undisturbed rocks and minerals—I: Water, chemical weathering, and atmospheric argon. *Geol. Soc. Am. Special Pap.* **430**, 285–303.

Ballmer M. D., Ito G., van Hunen J. and Tackley P. J. (2011) Spatial and temporal variability in Hawaiian hotspot volcanism induced by small-scale convection. *Nat. Geosci.* **4**, 457–460.

Ballmer M. D., Schumacher L., Lekic V., Thomas C. and Ito G. (2016) Compositional layering within the large low shear-wave velocity provinces in the lower mantle. *Geochem. Geophys. Geosyst.* **17**, 5056–5077.

Bianco T. A., Ito G., van Hunen J., Ballmer M. D. and Mahoney J. J. (2008) Geochemical variation at the Hawaiian hot spot caused by upper mantle dynamics and melting of a heterogeneous plume. *Geochem. Geophys. Geosyst.* **9**, Q11003.

Bianco T. A., Ito G., van Hunen J., Ballmer M. D. and Mahoney J. J. (2011) Geochemical variations at intraplate hot spots caused by variable melting of a veined mantle plume. *Geochem. Geophys. Geosyst.* **12**, Q0AC13.

Blichert-Toft J., Weis D., Maerschalk C., Agranier A. and Albarède F. (2003) *Hawaiian hot spot dynamics as inferred from the Hf and Pb isotope evolution of Mauna Kea volcano* Geochem. Geophys. Geosyst., 4.

Bryce J. G., DePaolo D. J. and Lassiter J. C. (2005) Geochemical structure of the Hawaiian plume: Sr, Nd, and Os isotopes in the 2.8 km HSDP-2 section of Mauna Kea volcano. *Geochem. Geophys. Geosyst.* **6**.

Burke K., Steinberger B., Torsvik T. H. and Smethurst M. A. (2008) Plume generation zones at the margins of large low shear velocity provinces on the core–mantle boundary. *Earth Planet. Sci. Lett.* **265**, 49–60.

Campbell I. H. (2007) Testing the plume theory. *Chem. Geol.* **241**, 153–176.

Chaffey D. J., Cliff R. A. and Wilson B. M. (1989) Characterization of the St. Helena magma source. *Magmatism in the Ocean Basins* **42**, 19.

Class C. and le Roex A. P. (2008) Ce anomalies in Gough Island lavas – Trace element characteristics of a recycled sediment component. *Earth Planet. Sci. Lett.* **265**, 475–486.

Class C. and le Roex A. (2011) South Atlantic DUPAL anomaly – Dynamic and compositional evidence against a recent shallow origin. *Earth Planet. Sci. Lett.* **305**, 92–102.

Class C. and Lehnert K. (2012) PetDB Expert MORB (Mid-Ocean Ridge Basalt) Compilation. *Interdisciplinary Earth Data Alliance (IEDA)*. https://doi.org/10.1594/IEDA/100060.

Cliff R. A., Baker P. E. and Mateer N. J. (1991) Geochemistry of inaccessible island volcanics. *Chem. Geol.* **92**, 251–260.

Cooper A. F. and Reid D. L. (1998) Nepheline Sövites as parental magmas in carbonatite complexes: evidence from Dicker Willem, Southwest Namibia. *J. Petrol.* **39**, 2123–2136.

Cooper A. F. and Reid D. L. (2000) The association of potassic trachytes and carbonatites at the Dicker Willem Complex, southwest Namibia: coexisting, immiscible, but not cogenetic magmas. *Contrib. Mineral. Petrol.* **139**, 570–583.

Courtillot V., Davaille A., Besse J. and Stock J. (2003) Three distinct types of hotspots in the Earth's mantle. *Earth Planet. Sci. Lett.* **205**, 295–308.

Davies G. R., Spriggs A. J. and Nixon P. H. (2001) A non-cognate origin for the Gibeon Kimberlite Megacryst Suite, Namibia: implications for the origin of Namibian Kimberlites. *J. Petrol.* **42**, 159–172.

Douglass J., Schilling J.-G. and Fontignie D. (1999) Plume-ridge interactions of the discovery and Shona mantle plumes with the southern Mid-Atlantic Ridge (40°-55°S). *J. Geophys. Res. Solid Earth* **104**, 2941–2962.

Eisele J., Abouchami W., Galer S. J. and Hofmann A. W. (2003) The 320 kyr Pb isotope evolution of Mauna Kea lavas recorded in the HSDP-2 drill core. *Geochem. Geophys. Geosyst.* **4**.

Escrig S., Schiano P., Schilling J.-G. and Allègre C. (2005) Rhenium–osmium isotope systematics in MORB from the Southern Mid-Atlantic Ridge (40°–50° S). *Earth Planet. Sci. Lett.* **235**, 528–548.

Fairhead J. D. and Wilson M. (2005) Plate tectonic processes in the South Atlantic Ocean: do we need deep mantle plumes? In *Plates, Plumes and Paradigms* (eds. G. R. Foulger, J. H. Natland, D. C. Presnall and D. L. Anderson). Geological Society of America.

Farnetani C. G. and Hofmann A. W. (2009) Dynamics and internal structure of a lower mantle plume conduit. *Earth Planet. Sci. Lett.* **282**, 314–322.

Farnetani C. G., Hofmann A. W. and Class C. (2012) How double volcanic chains sample geochemical anomalies from the lowermost mantle. *Earth Planet. Sci. Lett.* **359–360**, 240–247.

Fontignie D. and Schilling J. G. (1996) Mantle heterogeneities beneath the South Atlantic: a Nd-Sr-Pb isotope study along the Mid-Atlantic Ridge (3°S-46°S). *Earth Planet. Sci. Lett.* **142**, 209–221.

Foulger G. R. (2018) Origin of the South Atlantic igneous province. *J. Volcanol. Geotherm. Res.* **355**, 2–20.

French S. W. and Romanowicz B. A. (2014) Whole-mantle radially anisotropic shear velocity structure from spectral-element waveform tomography. *Geophys. J. Int.* **199**, 1303–1327.

French S. W. and Romanowicz B. (2015) Broad plumes rooted at the base of the Earth's mantle beneath major hotspots. *Nature* **525**, 95–99.

Garcia M. O., Swinnard L., Weis D., Greene A. R., Tagami T., Sano H. and Gandy C. E. (2010) Petrology, geochemistry and geochronology of Kaua'i Lavas over 4·5 Myr: implications for the origin of rejuvenated volcanism and the evolution of the Hawaiian Plume. *J. Petrol.* **51**, 1507–1540.

Garnero E. J. and McNamara A. K. (2008) Structure and dynamics of Earth's lower mantle. *Science* **320**, 626–628.

Geldmacher J., Hoernle K., Klügel A., van den Bogaard P. and Bindeman I. (2008) Geochemistry of a new enriched mantle type locality in the northern hemisphere: implications for the origin of the EM-I source. *Earth Planet. Sci. Lett.* **265**, 167–182.

Gibson S. A., Thompson R. N., Day J. A., Humphris S. E. and Dickin A. P. (2005) Melt-generation processes associated with the Tristan mantle plume: Constraints on the origin of EM-1. *Earth Planet. Sci. Lett.* **237**, 744–767.

Hanan B. B., Kingsley R. H. and Schilling J. G. (1986) Pb isotope evidence in the South Atlantic for migrating ridge-hotspot interactions. *Nature* **322**, 137–144.

Hanan B. B. and Graham D. W. (1996) Lead and helium isotope evidence from oceanic basalts for a common deep source of mantle plumes. *Science* **272**, 991–995.

Hanyu T., Kawabata H., Tatsumi Y., Kimura J.-I., Hyodo H., Sato K., Miyazaki T., Chang Q., Hirahara Y., Takahashi T., Senda R. and Nakai S. i. (2014) sotope evolution in the HIMU reservoir beneath St. Helena: Implications for the mantle recycling of U and Th. *Geochim. Cosmochim. Acta* **143**, 232–252.

Harpp K. S. and White W. M. (2001) Tracing a mantle plume: isotopic and trace element variations of Galápagos seamounts. *Geochem. Geophys. Geosyst.* **2**.

Harpp K. S., Hall P. S. and Jackson M. G. (2014) Galápagos and Easter: a tale of two hotspots. *The Galápagos: A natural laboratory for the Earth Sciences* **204**, 27–40.

Harrison L. N., Weis D. and Garcia M. O. (2017) The link between Hawaiian mantle plume composition, magmatic flux, and deep mantle geodynamics. *Earth Planet. Sci. Lett.* **463**, 298–309.

Hart S. R. (1984) A large-scale isotope anomaly in the Southern Hemisphere mantle. *Nature* **309**, 753–757.

Hart S. R., Hauri E. H., Oschmann L. A. and Whitehead J. A. (1992) Mantle Plumes and Entrainment: Isotopic Evidence. *Science* **256**, 517–520.

Hauff F., Hoernle K., Tilton G., Graham D. W. and Kerr A. C. (2000) Large volume recycling of oceanic lithosphere over short time scales: geochemical constraints from the Caribbean Large Igneous Province. *Earth Planet. Sci. Lett.* **174**, 247–263.

Hicks A., Barclay J., Mark D. F. and Loughlin S. (2012) Tristan da Cunha: constraining eruptive behavior using the 40Ar/39Ar dating technique. *Geology* **40**, 723–726.

Hoernle K. and Schmincke H.-U. (1993) The role of partial melting in the 15 Ma geochemical evolution of Gran Canaria: a Blob model for the Canary Hotspot. *J. Petrol.* **34**, 599–626.

Hoernle K., Werner R., Morgan J. P., Garbe-Schönberg D., Bryce J. and Mrazek J. (2000) Existence of complex spatial zonation in the Galápagos plume. *Geology* **28**, 435–438.

Hoernle, K., Werner, R. and Lüter, C. (2014) RV SONNE Fahrtbericht/Cruise Report SO233 WALVIS II, 14.05-21.06.

2014, Cape Town, South Africa-Walvis Bay, Namibia. GEOMAR Report no. 23 (N. Ser.), 53 pp + Appendices. https://doi.org/10.3289/GEOMAR_REP_NS_22_2014.

Hoernle K., Rohde J., Hauff F., Garbe-Schonberg D., Homrighausen S., Werner R. and Morgan J. P. (2015) How and when plume zonation appeared during the 132 Myr evolution of the Tristan Hotspot. *Nat. Commun.* **6**. https://doi.org/10.1038/ncomms8799.

Hoernle K., Schwindrofska A., Werner R., van den Bogaard P., Hauff F., Uenzelmann-Neben G. and Garbe-Schönberg D. (2016) Tectonic dissection and displacement of parts of Shona hotspot volcano 3500 km along the Agulhas-Falkland Fracture Zone. *Geology* **44**, 263–266.

Hofmann A. W. (1988) Chemical differentiation of the earth - the relationship between mantle, continental crust, and oceanic crust. *Earth Planet. Sci. Lett.* **90**, 297–314.

Hofmann A. W. and Farnetani C. G. (2013) Two views of Hawaiian plume structure. *Geochem. Geophys. Geosyst.* **14**, 5308–5322.

Homrighausen S., Hoernle K., Geldmacher J., Wartho J. A., Hauff F., Portnyagin M., Werner R., van den Bogaard P. and Garbe-Schönberg D. (2018a) Unexpected HIMU-type late-stage volcanism on the Walvis Ridge. *Earth Planet. Sci. Lett.* **492**, 251–263.

Homrighausen S., Hoernle K., Hauff F., Geldmacher J., Wartho J.-A., van den Bogaard P. and Garbe-Schönberg D. (2018b) Global distribution of the HIMU end member: formation through Archean plume-lid tectonics. *Earth-Sci. Rev.* **182**, 85–101.

Huang S., Hall P. S. and Jackson M. G. (2011) Geochemical zoning of volcanic chains associated with Pacific hotspots. *Nat. Geosci.* **4**, 874–878.

Humphris S. E. and Thompson G. (1983) Geochemistry of rare earth elements in basalts from the Walvis Ridge: implications for its origin and evolution. *Earth Planet. Sci. Lett.* **66**, 223–242.

Ingle S., Weis D. and Frey F. A. (2002) Indian continental crust recovered from Elan Bank, Kerguelen Plateau (ODP Leg 183, Site 1137). *J. Petrol.* **43**, 1241–1257.

Janney P. E., Le Roex A. P., Carlson R. W. and Viljoen K. S. (2002) A chemical and multi-isotope study of the Western Cape Olivine Melilitite Province, South Africa: implications for the sources of Kimberlites and the Origin of the HIMU Signature in Africa. *J. Petrol.* **43**, 2339–2370.

Jochum K. P. and Verma S. P. (1996) Extreme enrichment of Sb, Tl and other trace elements in altered MORB. *Chem. Geol.* **130**, 289–299.

Jones C. E. and Jenkyns H. C. (2001) Seawater strontium isotopes, oceanic anoxic events, and seafloor hydrothermal activity in the Jurassic and Cretaceous. *Am. J. Sci.* **301**, 112–149.

Jones T. D., Davies D. R., Campbell I. H., Wilson C. R. and Kramer S. C. (2016) Do mantle plumes preserve the heterogeneous structure of their deep-mantle source? *Earth Planet. Sci. Lett.* **434**, 10–17.

Jones T. D., Davies D. R., Campbell I. H., Iaffaldano G., Yaxley G., Kramer S. C. and Wilson C. R. (2017) The concurrent emergence and causes of double volcanic hotspot tracks on the Pacific plate. *Nature* **545**, 472.

Kawabata H., Hanyu T., Chang Q., Kimura J.-I., Nichols A. R. L. and Tatsumi Y. (2011) The petrology and geochemistry of St. Helena alkali basalts: evaluation of the oceanic crust-recycling model for HIMU OIB. *J. Petrol.* **52**, 791–838.

Kerr R. C. and Mériaux C. (2004) Structure and dynamics of sheared mantle plumes. *Geochem. Geophys. Geosyst.* **5**.

Kurz M. D., Jenkins W. J. and Hart S. R. (1982) Helium isotopic systematics of oceanic islands and mantle heterogeneity. *Nature* **297**, 43–47.

Kurz M. D., le Roex A. P. and Dick H. J. B. (1998) Isotope geochemistry of the oceanic mantle near the Bouvet triple junction. *Geochim. Cosmochim. Acta* **62**, 841–852.

Kurz M. D., Curtice J., Lott D. E. and Solow A. (2004) Rapid helium isotopic variability in Mauna Kea shield lavas from the Hawaiian scientific drilling project. *Geochem. Geophys. Geosyst.* **5**.

Le Maitre R. W. (1962) Petrology of volcanic rocks, Gough Island, South Atlantic. *Geol. Soc. Am. Bull.* **73**, 1309–1340.

Le Roex A., Class C., O'Connor J. and Jokat W. (2010) Shona and discovery aseismic ridge systems, South Atlantic: trace element evidence for enriched mantle sources. *J. Petrol.* **51**, 2089–2120.

Le Roex A. P. (1985) Geochemistry, mineralogy and magmatic evolution of the Basaltic and Trachytic Lavas from Gough Island, South Atlantic. *J. Petrol.* **26**, 149–186.

Le Roex A. P., Dick H. J. B., Reid A. M., Frey F. A., Erlank A. J. and Hart S. R. (1985) Petrology and geochemistry of basalts from the American-Antarctic Ridge, Southern Ocean: implications for the westward influence of the Bouvet mantle plume. *Contrib. Mineral. Petr.* **90**, 367–380.

Le Roex A. P., Cliff R. A. and Adair B. J. I. (1990) Tristan da Cunha, South Atlantic: geochemistry and petrogenesis of a Basanite-Phonolite Lava Series. *J. Petrol.* **31**, 779–812.

le Roux P. J., le Roex A. P., Schilling J. G., Shimizu N., Perkins W. W. and Pearce N. J. G. (2002) Mantle heterogeneity beneath the southern Mid-Atlantic Ridge: trace element evidence for contamination of ambient asthenospheric mantle. *Earth Planet. Sci. Lett.* **203**, 479–498.

Li M., McNamara A. K. and Garnero E. J. (2014) Chemical complexity of hotspots caused by cycling oceanic crust through mantle reservoirs. *Nat. Geosci.* **7**, 366–370.

Lohmann F. C., Hort M. and Phipps Morgan J. (2009) Flood basalts and ocean island basalts: a deep source or shallow entrainment? *Earth Planet. Sci. Lett.* **284**, 553–563.

Luchs T., Brey G. P., Gerdes A. and Höfer H. E. (2013) The lithospheric mantle underneath the Gibeon Kimberlite field (Namibia): a mix of old and young components—Evidence from Lu–Hf and Sm–Nd isotope systematics. *Precambr. Res.* **231**, 263–276.

Maund J. G., Rex D. C., Le Roex A. P. and Reid D. L. (1988) Volcanism on Gough Island: a revised stratigraphy. *Geol. Mag.* **125**, 175–181.

McNamara A. K., Garnero E. J. and Rost S. (2010) Tracking deep mantle reservoirs with ultra-low velocity zones. *Earth Planet. Sci. Lett.* **299**, 1–9.

Montelli R., Nolet G., Dahlen F. A. and Masters G. (2006) A catalogue of deep mantle plumes: new results from finite-frequency tomography. *Geochem. Geophys. Geosyst.* **7**, Q11007.

Morgan W. J. (1971) Convection plumes in the lower Mantle. *Nature* **230**, 42–43.

Morgan W. J. (1981) 13. Hotspot tracks and the opening of the Atlantic and Indian Oceans. *Oceanic Lithosphere* **7**, 443.

Nobre Silva I. G., Weis D., Scoates J. S. and Barling J. (2013) The Ninetyeast ridge and its relation to the Kerguelen, Amsterdam and St. Paul Hotspots in the Indian Ocean. *J. Petrol.* **54**, 1177–1210.

O'Connor J. M. and Duncan R. A. (1990) Evolution of the Walvis ridge-rio grande rise hot spot system: implications for African and South American plate motions over plumes. *J. Geophys. Res. Solid Earth* **95**, 17475–17502.

O'Connor J. M. and le Roex A. P. (1992) South Atlantic hot spot-plume systems: 1. Distribution of volcanism in time and space. *Earth Planet. Sci. Lett.* **113**, 343–364.

O'Connor J. M., Jokat W., le Roex A. P., Class C., Wijbrans J. R., Keszling S., Kuiper K. F. and Nebel O. (2012) Hotspot trails in

the South Atlantic controlled by plume and plate tectonic processes. *Nat. Geosci.* **5**, 735–738.
O'Connor J. M. and Jokat W. (2015a) Tracking the Tristan-Gough mantle plume using discrete chains of intraplate volcanic centers buried in the Walvis Ridge. *Geology* **43**, 715–718.
O'Connor J. M. and Jokat W. (2015b) Age distribution of Ocean Drill sites across the Central Walvis Ridge indicates plate boundary control of plume volcanism in the South Atlantic. *Earth Planet. Sci. Lett.* **424**, 179–190.
Pearce J. A. (1996) A user's guide to basalt discrimination diagrams. Trace element geochemistry of volcanic rocks: applications for massive sulphide exploration. *Geological Association of Canada, Short Course Notes* **12**, 113.
Pearce J. A. (2008) Geochemical fingerprinting of oceanic basalts with applications to ophiolite classification and the search for Archean oceanic crust. *Lithos* **100**, 14–48.
Renne P. (2015) Age and duration of the paraná-etendeka flood basalts and related plumbing system. In: AGU Fall Meeting Abstracts.
Renne P. R., Glen J. M., Milner S. C. and Duncan A. R. (1996) Age of Etendeka flood volcanism and associated intrusions in southwestern Africa. *Geology* **24**, 659–662.
Rhodes J. and Vollinger M. (2004) Composition of basaltic lavas sampled by phase-2 of the Hawaii Scientific drilling project: geochemical stratigraphy and magma types. *Geochem. Geophys. Geosyst.* **5**.
Richards M. A., Duncan R. A. and Courtillot V. E. (1989) Flood basalts and hot-spot tracks: plume heads and tails. *Science* **246**, 103–107.
Richardson S., Erlank A., Reid D. and Duncan A. (1984) Major and trace-elements and Nd and Sr isotope geochemistry of basalts from the deep-sea drilling project LEG-74 Walvis ridge transect. *Init. Rep. Deep Sea Drilling Proj.* **74**, 739–754.
Richardson S. H., Erlank A. J., Duncan A. R. and Reid D. L. (1982) Correlated Nd, Sr and Pb Isotope Variation in Walvis Ridge Basalts and Implications for the Evolution of their Mantle Source. *Earth Planet. Sci. Lett.* **59**, 327–342.
Rohde J., Hoernle K., Hauff F., Werner R., O'Connor J., Class C., Garbe-Schönberg D. and Jokat W. (2013a) 70 Ma chemical zonation of the Tristan-Gough hotspot track. *Geology* **43**, 335–338.
Rohde J. K., van den Bogaard P., Hoernle K., Hauff F. and Werner R. (2013b) Evidence for an age progression along the Tristan-Gough volcanic track from new 40Ar/39Ar ages on phenocryst phases. *Tectonophysics* **604**, 60–71.
Salters V. J. M. and Sachi-Kocher A. (2010) An ancient metasomatic source for the Walvis Ridge basalts. *Chem. Geol.* **273**, 151–167.
Salters V. J. M., Mallick S., Hart S. R., Langmuir C. E. and Stracke A. (2011) Domains of depleted mantle: new evidence from hafnium and neodymium isotopes. *Geochem. Geophys. Geosyst.* **12**, n/a-n/a.
Sarda P., Moreira M., Staudacher T., Schilling J.-G. and Allègre C. J. (2000) Rare gas systematics on the southernmost Mid-Atlantic Ridge: constraints on the lower mantle and the Dupal source. *J. Geophys. Res. Solid Earth* **105**, 5973–5996.
Schilling J. G., Hanan B. B., McCully B., Kingsley R. H. and Fontignie D. (1994) Influence of the Sierra Leone mantle plume on the equatorial Mid-Atlantic Ridge: A Nd-Sr-Pb isotopic study. *J. Geophys. Res. Solid Earth* **99**, 12005–12028.
Schlömer A., Geissler W. H., Jokat W. and Jegen M. (2017) Hunting for the Tristan mantle plume – An upper mantle tomography around the volcanic island of Tristan da Cunha. *Earth Planet. Sci. Lett.* **462**, 122–131.
Schwindrofska A., Hoernle K., Hauff F., van den Bogaard P., Werner R. and Garbe-Schönberg D. (2016) Origin of enriched components in the South Atlantic: evidence from 40 Ma geochemical zonation of the Discovery Seamounts. *Earth Planet. Sci. Lett.* **441**, 167–177.
Steinberger B. and Torsvik T. H. (2012) A geodynamic model of plumes from the margins of Large Low Shear Velocity Provinces. *Geochem. Geophys. Geosyst.* **13**, Q01W09.
Stracke A., Hofmann A. W. and Hart S. R. (2005) FOZO, HIMU, and the rest of the mantle zoo. *Geochem. Geophys. Geosyst.* **6**, Q05007.
Stracke A. (2012) Earth's heterogeneous mantle: a product of convection-driven interaction between crust and mantle. *Chem. Geol.* **330–331**, 274–299.
Stroncik N. A., Trumbull R. B., Krienitz M.-S., Niedermann S., Romer R. L., Harris C. and Day J. (2017) Helium isotope evidence for a deep-seated mantle plume involved in South Atlantic breakup. *Geology* **45**, 827–830.
Suetsugu D., Isse T., Tanaka S., Obayashi M., Shiobara H., Sugioka H., Kanazawa T., Fukao Y., Barruol G. and Reymond D. (2009) South Pacific mantle plumes imaged by seismic observation on islands and seafloor. *Geochem. Geophys. Geosyst.* **10**.
Sun S.-S. (1980) The evidence for chemical heterogeneity in the Earth's mantle - Lead isotopic study of young volcanic rocks from mid-ocean ridges, ocean islands and island arcs. *Philos. Trans. Roy. Soc. London Ser. A, Math. Phys. Sci.* **297**, 409–445.
Thompson G. and Humphris S. (1984) Petrology and geochemistry of rocks from the Walvis Ridge-Deep-Sea Drilling Project Leg-74, Site525, Site527 and Site528. *Init. Rep. Deep Sea Drilling Proj.* **74**, 755–764.
Thorne M. S., Garnero E. J. and Grand S. P. (2004) Geographic correlation between hot spots and deep mantle lateral shear-wave velocity gradients. *Phys. Earth Planet. Inter.* **146**, 47–63.
Torsvik T. H., Smethurst M. A., Burke K. and Steinberger B. (2006) Large igneous provinces generated from the margins of the large low-velocity provinces in the deep mantle. *Geophys. J. Int.* **167**, 1447–1460.
Torsvik T. H., Burke K., Steinberger B., Webb S. J. and Ashwal L. D. (2010) Diamonds sampled by plumes from the core-mantle boundary. *Nature* **466**, 352–355.
Torsvik T. H., Van der Voo R., Preeden U., Mac Niocaill C., Steinberger B., Doubrovine P. V., van Hinsbergen D. J. J., Domeier M., Gaina C., Tohver E., Meert J. G., McCausland P. J. A. and Cocks L. R. M. (2012) Phanerozoic polar wander, palaeogeography and dynamics. *Earth-Sci. Rev.* **114**, 325–368.
van den Bogaard P. (2013) The origin of the Canary Island Seamount Province - New ages of old seamounts. *Sci. Rep.* **3**, 2107.
Wang X.-C., Li Z.-X., Li X.-H., Li J., Xu Y.-G. and Li X.-H. (2013) Identification of an ancient mantle reservoir and young recycled materials in the source region of a young mantle plume: implications for potential linkages between plume and plate tectonics. *Earth Planet. Sci. Lett.* **377**, 248–259.
Weaver B. L., Wood D. A., Tarney J. and Joron J. L. (1987) Geochemistry of ocean island basalts from the South Atlantic: Ascension, Bouvet, St. Helena, Gough and Tristan da Cunha. *Geol. Soc. London, Special Publ.* **30**, 253–267.
Weis D., Garcia M. O., Rhodes J. M., Jellinek M. and Scoates J. S. (2011) Role of the deep mantle in generating the compositional asymmetry of the Hawaiian mantle plume. *Nat. Geosci.* **4**, 831–838.
Weit A., Trumbull R. B., Keiding J. K., Geissler W. H., Gibson S. A. and Veksler I. V. (2017) The magmatic system beneath the Tristan da Cunha Island: Insights from thermobarometry, melting models and geophysics. *Tectonophysics* **716**, 64–76.
Werner R., Hoernle K., Barckhausen U. and Hauff F. (2003) Geodynamic evolution of the Galápagos hot spot system

(Central East Pacific) over the past 20 my: Constraints from morphology, geochemistry, and magnetic anomalies. *Geochem. Geophys. Geosyst.*, 4.

Werner R. and Wagner H. -J. (2014) RV SONNE Fahrtbericht/ Cruise Report SO234/1 "SPACES": Science or the Assessment of Complex Earth System Processes, 22.06.–06.07. 2014, Walvis Bay/Namibia-Durban/South Africa. GEOMAR Report no. 17 (N. Ser.), 29 pp + Appendices. https://doi.org/10.3289/GEOMAR_REP_NS_17_2014

Willbold M. and Stracke A. (2006) Trace element composition of mantle end-members: Implications for recycling of oceanic and upper and lower continental crust. *Geochem. Geophys. Geosyst.* **7**, Q04004.

Willbold M. and Stracke A. (2010) Formation of enriched mantle components by recycling of upper and lower continental crust. *Chem. Geol.* **276**, 188–197.

Wilson J. T. (1963) Evidence from Islands on the Spreading of Ocean Floors. *Nature* **197**, 536–538.

Wilson J. T. (1973) Mantle plumes and plate motions. *Tectonophysics* **19**, 149–164.

Wörner G., Zindler A., Staudigel H. and Schmincke H. U. (1986) Sr, Nd, and Pb isotope geochemistry of Tertiary and Quaternary alkaline volcanics from West Germany. *Earth Planet. Sci. Lett.* **79**, 107–119.

Zhao D. (2007) Seismic images under 60 hotspots: Search for mantle plumes. *Gondwana Res.* **12**, 335–355.

Zindler A. and Hart S. R. (1986) Chemical geodynamics. *Annu. Rev. Earth Planet. Sci.* **14**, 493–571.

FURTHER READING

Bianco T. A., Ito G., Becker J. M. and Garcia M. O. (2005) Secondary Hawaiian volcanism formed by flexural arch decompression. *Geochem. Geophys. Geosyst.* **6**, Q08009.

Associate Editor: Andreas Stracke